frontiers in Marine Science

ORIGINAL RESEARCH
published: 09 June 2020
doi: 10.3389/fmars.2020.00410

Nitrogen Deprivation-Induced Production of Volatile Organic Compounds in the Arachidonic-Acid-Accumulating Microalga *Lobosphaera incisa* Underpins Their Role as ROS Scavengers and Chemical Messengers

*Puja Kumari†, Alon Cna'ani, Shoshana Didi-Cohen, Vered Tzin and Inna Khozin-Goldberg**

French Associates Institute for Agriculture and Biotechnology of Drylands, Jacob Blaustein Institutes for Desert Research, Ben-Gurion University of the Negev, Beersheba, Israel

OPEN ACCESS

Edited by:
Yuji Hiwatashi, Miyagi University, Japan

Reviewed by:
Susana Puntarulo, University of Buenos Aires, Argentina
Tiziano Verri, University of Salento, Italy

***Correspondence:**
Inna Khozin-Goldberg
khozin@bgu.ac.il

†Present address:
Puja Kumari, Faculty of Fisheries Sciences, Hokkaido University, Hakodate, Japan

Specialty section:
This article was submitted to Aquatic Physiology, a section of the journal Frontiers in Marine Science

Received: *31 March 2020*
Accepted: *12 May 2020*
Published: *09 June 2020*

Citation:
Kumari P, Cna'ani A, Didi-Cohen S, Tzin V and Khozin-Goldberg I (2020) Nitrogen Deprivation-Induced Production of Volatile Organic Compounds in the Arachidonic-Acid-Accumulating Microalga Lobosphaera incisa Underpins Their Role as ROS Scavengers and Chemical Messengers. Front. Mar. Sci. 7:410. doi: 10.3389/fmars.2020.00410

The green microalga *Lobosphaera incisa* accumulates long-chain polyunsaturated arachidonic acid sequestered in triacylglycerols under nitrogen (N)-starvation conditions. Many of *L. incisa*'s physiological and metabolic responses to N-starvation have been previously investigated. However, the temporal dynamics of the volatile organic compounds (VOCs) under different N availability and their role in *L. incisa* stress responses have yet to be elucidated. Here, we investigated the VOC profiles of *L. incisa* to reveal their emission patterns, and proposed their physiological roles under N-starvation. Using gas chromatography-mass spectrometry, 42 and 19 VOCs were identified in the algal biomass (AVOCs) and in the medium (MVOCs), respectively, belonging to alkanes, alkenes, benzenoids, esters, fatty alcohols, fatty aldehydes, fatty acids (FAs), FA esters, ketones, and terpenoids; most of these are the oxidative products of FAs or photosynthetic pigment degradation. The discriminant AVOCs and MVOCs produced under N-starvation were identified by principal component analyses and hierarchical clustering. A significant treatment- and time-dependent increase in volatile FAs and their oxidative products was observed in the algal biomass and medium under N-starvation as compared to N-replete controls, following a similar pattern as reactive oxygen species (ROS) production. This suggests that VOCs may be involved in ROS scavenging. Despite the increase in total VOCs, terpenoids and alkenes decreased significantly with N-starvation duration, along with chloroplast degradation. Transcriptomics data supported the VOC patterns and revealed the upregulation of genes involved in fatty aldehyde, fatty alcohol, and ketone synthesis, including lipoxygenase, thioesterase, and fatty acyl CoA reductase, along with a decrease in

the expression of genes putatively implicated in alkene biosynthesis. Several VOCs were identified as potential biotechnological targets, and their putative biosynthetic pathways were proposed, which could be genetically manipulated to enhance the yields of high value products. We conclude that VOCs may play an important role in stress metabolism, ROS scavenging, and the amelioration of oxidative stress under N-starvation. Also, VOCs released in the medium may communicate the signal to neighboring cells, thus priming them to adjust their metabolic activities to adapt to N-starvation conditions, indicating that the function of VOCs as chemical signaling messengers is conserved from microalgae to higher plants.

Keywords: *Lobosphaera incisa*, lipoxygenase, nitrogen stress, polyunsaturated aldehydes, reactive oxygen species, volatiles

INTRODUCTION

Microalgae constitute a diverse group of predominantly photosynthetic and aquatic eukaryotic microorganisms, with high ecophysiological and biotechnological significance. Microalgae, particularly planktonic species, are known to produce a variety of volatile organic compounds (VOCs) with important roles in ecology, atmospheric chemistry, and global climate. VOCs comprise low molecular weight compounds with low to moderate hydrophilicity and high vapor pressure at ambient conditions (20°C and 101.3 kPa). The dispersal of VOCs at the air-water interface facilitates their infochemical effects on both terrestrial and aquatic organisms. Infochemicals are chemical cues emitted or secreted by organisms that influence ecological interactions in nature. The VOC metabolic profile of an organism has been termed "volatilome" (or "volatome"), and the respective field of study is called volatilomics (Achyuthan et al., 2017).

Studies on the volatilomes of cultivated microalgal species is still in its infancy. VOCs produced by microalgae are known to include volatile aldehydes, alcohols, esters, carboxylic acids, hydrocarbons, ketones, furans, fatty acids derived from lipid metabolic pathways, carotenoid and terpene derivatives (ionones, cyclocitrals), sulfur, and halogenated compounds (Santos et al., 2016; Achyuthan et al., 2017; Zhou et al., 2017; Hosoglu, 2018). The emission of VOCs in microalgal cultures can vary across different species and is affected by environmental conditions. Both abiotic and biotic factors elicit VOC generation in microalgal cultures, such as temperature, light, nutrients, pH, salinity, oxidative stress, wounding, and predators (Achyuthan et al., 2017). Furthermore, the VOC emission spectra may be species- and condition-specific, hence serving as useful biomarkers of culture stage, health, performance, and the presence of predators. In addition, VOCs hold promise as high-value by-products with a range of applications in the food and biofuels industry (Achyuthan et al., 2017). VOCs are considered to be the main by-products formed during growth under phototrophic conditions and may represent up to 90% of the total carbon substrate converted in the photobioreactor, as indicated by a carbon balance analysis (Jacob-Lopes and Franco, 2013). Understanding the mechanisms underlying VOC emission and characterizing the volatile fraction can establish routes for the bioconversion of desired substrates, enabling potential applications of the volatile molecules (Jacob-Lopes et al., 2010; Jacob-Lopes and Franco, 2013). Despite diversity and importance of microalgal VOCs, little quantitative or genetic information is available on VOC biogeneration *in vivo* or on their biochemistry and environmental impact, in particular by green microalgae (Chlorophyta), as compared to higher plants, phytoplankton, and macroalgae.

Plant volatiles (especially C6 aldehydes and alcohols, called green leaf volatiles) are involved in plant-herbivore tritrophic and intraspecific interactions. They also play a role in pollination, and communications within and between plant communities (Kihara et al., 2014; Ameye et al., 2018). In marine systems, macroalgae-derived volatiles, mainly represented by organic halogens, aldehydes, and dimethyl sulfide, are involved in defense and trophic interactions (Jerković et al., 2018; Song et al., 2018; Zhu et al., 2018). Phytoplankton-derived VOCs are known for the eco-physiological roles they play in the aquatic environment, acting as info(semio)chemicals in intraspecific (pheromones) and interspecific (kairomones) communication, predator-prey interactions, activated defenses, interspecific non-communicative interactions, mainly involving dimethyl sulfide, dimethylsulfoniopropionate and short-chain polyunsaturated aldehydes (PUAs), and their

Abbreviations: ALA, α-linolenic acid; ANOVA, One-way analysis of variance; ARA, arachidonic acid; AVOCs, VOCs identified in algal biomass; Car, carotenoids; CER 1, eceriferum 1; Chl, chlorophyll; DCF- 2′,7′, dichlorofluorescein; DCF-FU, 2′;7′-dichlorofluorescein fluorescent unit; DCFH-DA, dichlorodihydrofluorescein diacetate; DW, dry weight; FA, fatty acid; FAME, fatty acid methyl esters; FAP, fatty acid photodecarboxylase; FAR, fatty acyl (CoA) ACP reductase; FID, flame ionization detector; GC-MS, gas chromatography mass spectrometry; GMC, glucose-methanol-choline oxidoreductase; HPETE, hydroperoxyeicosatetraenoic acid; HPL, hydroperoxide lyase; HPOT, hydroperoxyoctadecadienoic acid; IBB, Isobutylbenzene; KAR, 3-ketoacyl-ACP reductase; LA, linoleic acid; LACS, long-chain acyl-CoA synthetase; LOX, lipoxygenase; MUFAs, monounsaturated fatty acids; MVOCs, VOCs identified in culture medium; OA, oleic acid; PCA, principal component analysis; PES, phytyl ester synthase; PGD1, plastid galactoglycerolipid degradation1; PUFA, polyunsaturated fatty acid; ROS, reactive oxygen species; SFAs, saturated fatty acids; SPME, solid-phase microextraction; TAG, triacylglycerol; TFA, total fatty acid; TVOCs, total volatile organic compound; VOCs, volatile organic compounds; Vol, volumetric.

enhancing of tolerance against biotic and abiotic stresses (Fink, 2007; Zuo et al., 2012a; Moelzner and Fink, 2015; Zuo, 2019).

Analyzing VOCs can provide useful information about the metabolic state of an algal culture. VOCs are known to be produced by microalgae, but little is known why microalgae are involved in energy-expensive VOC production and release. There is limited information on the physiological significance of microalgal VOC emissions in cultivated species in response to environmental stresses. In particular, the role of VOC emission in the microalgal response to nutrient starvation, an approach commonly applied in biotechnology to induce storage product accumulation, is little studied. In this work, we investigated VOC profiles and dynamics in the cultures of the green microalga *Lobosphaera incisa*. This microalga is a promising photosynthetic source of long-chain polyunsaturated fatty acid (LC-PUFA) arachidonic acid (ARA, 20:4*n*6), which is sequestered in storage lipid triacylglycerols under nitrogen (N)-starvation conditions. The ability to accumulate high amounts of LC-PUFA in storage lipids is not common in microalgae. Given its peculiar and unique fatty acid (FA) profile, *L. incisa* offers an attractive model in which to study VOC generation under stress conditions. Previous studies indicated that N-starvation triggers chloroplast degradation and reactive oxygen species (ROS) production, and enhances catabolic processes to sustain the ARA-rich triacylglycerol biosynthesis (Pal-Nath et al., 2017; Kokabi et al., 2019). Nevertheless, the production and the significance of VOCs generated under such stress conditions have not been investigated.

To elucidate whether VOC diversity and composition could be associated with the FA accumulation patterns in *L. incisa* and the magnitude of N-starvation-mediated cellular stress events, we analyzed, for the first time, the dynamics of VOC generation in the time-course of N-starvation conditions. We also identified molecules of possible commercial value and proposed their biogenic precursors and putative pathways in *L. incisa*. The results suggest that inducing VOC production may serve as a survival strategy for this microalga, achieved by broadcasting volatile signals to neighboring cells that most likely induce metabolic changes to cope with imminent N-starvation conditions.

MATERIALS AND METHODS

Algal Culture Conditions and Experimental Set-Up

The wild-type (WT) strain of *L. incisa* (deposited as SAG 2468 in the SAG Culture Collection of Microalgae) maintained in our laboratory was used for this study. *L. incisa* was cultivated in a complete modified BG-11 (+N mBG-11) and N-depleted medium (−N mBG-11 without nitrogen source $NaNO_3$) in 1-L glass columns (6.0 cm internal diameter), placed in a temperature-regulated water bath at 25°C, and bubbled with a mixture of 2% CO_2 in air (v/v), as described in Pal-Nath et al. (2017). Continuous illumination (170 μmol photons m^{-2} s^{-1}) was provided by white fluorescent lamps external to the water bath. To induce N starvation, algal cells in log phase were harvested by centrifugation at 3,000 × *g* for 5 min, washed twice in double-distilled water, resuspended in 600 mL of mBG-11 to a chlorophyll (Chl) concentration of 15 μg mL^{-1} for the control and 600 mL of N-depleted mBG-11 (Chl concentration of 30 μg mL^{-1}) for inducing N-starvation, and cultivated in triplicate columns for 14 days. Aliquots of algal culture (75 mL) were sampled during the experiment from the control and N-starved (-N) cultures on days 0, 1, 3, 6, and 14 for multiple measurements: Chl, total carotenoids (Car), dry weight (DW), reactive oxygen species (ROS), fatty acids (FAs), and VOC determination. The samples for all the above-mentioned parameters were processed the same day, except for FA analysis, for which the samples were freeze-dried and stored at −20°C.

Culture Growth Estimation

The growth of *L. incisa* cultures was estimated based on the volumetric content of Chl ($_{a+b}$) and on DW measurements (Pal-Nath et al., 2017) because this alga forms cell clusters, hindering cell counting. Briefly, Chl and total Car contents in the cultures were determined spectrophotometrically in dimethyl sulfoxide (DMSO) extracts, using a Cary 50 Bio spectrophotometer (Varian, United States) (Solovchenko et al., 2013). For DW determination, 5 ml of algal culture was diluted 2-fold with double-distilled water and filtered through pre-weighed 47-mm glass fiber paper filters (Whatman® GF/C, Schleicher & Schuell Co.). Filters were then dried in a microwave oven to constant weight, and dry weight was determined.

Fatty Acid (FA) Composition

The FA composition and content of the biomass were determined by a direct transmethylation procedure as previously described (Pal-Nath et al., 2011). Briefly, freeze-dried algal biomass (10 mg) in triplicates were incubated in dry methanol containing 2% (v/v) H_2SO_4 in glass vials at 80°C for 1.5 h under an argon atmosphere with continuous stirring. Heptadecanoic acid (C17:0) (Sigma-Aldrich) was added as an internal standard. The transmethylation reactions were terminated by cooling, and adding 1 ml of H_2O. Fatty acid methyl esters (FAMEs) were extracted with hexane and injected to GC-FID. FAMEs were quantified on a Trace GC Ultra (Thermo, Italy) equipped with a flame ionization detector (FID) and a programmed temperature vaporizing (PTV) injector. The detector temperature was fixed at 280°C, with a split ratio of 1:100, and helium was used as a carrier gas at a 2.5-ml min^{-1} flow rate. The PTV injector was programmed to increase the temperature from 40°C at the time of injection to 300°C at the time of sample transfer. The separation was achieved on a fused silica capillary column (SUPELCOWAX® 10, Sigma-Aldrich, 30 m × 0.32 mm) using the following oven temperature program: 1 min at 130°C, followed by a linear gradient to 220°C and finally 10 min isocratic at 220°C. FAMEs were identified by co-chromatography with authentic standards (Sigma-Aldrich).

Reactive Oxygen Species (ROS) Estimation

The ROS levels were measured by using 2′,7′-dichlorodihydrofluorescein diacetate (DCFH-DA) according to the method modified after Wang et al. (2011). The cell-penetrating DCFH-DA is hydrolyzed by intracellular esterases to form the nonfluorescent 2′,7′-DCFH and transformed to highly fluorescent 2′,7′-dichlorofluorescein (DCF) in the presence of free radicals and heme proteins, such as hydroxyl radical (OH) and H_2O_2-peroxidase (Halliwell and Gutteridge, 1999). However, there are known caveats associated with the DCF assay for ROS detection since it also reacts with reactive nitrogen species (RNS) (Kalyanaraman et al., 2012). A 10 mM stock solution of DCFH-DA was prepared in DMSO and stored at −20°C, and a 5 mM working solution was prepared each time from the stock prior to use. Then, 250 μl of algal culture (triplicates) was harvested by centrifuging at 1500 × *g* for 2 min, and the algal pellet was washed with mBG-11 for control samples and −N mBG-11 for nitrogen-starved samples, and re-suspended in 250 μl of the respective media in 1.5-ml tubes. Then, 5 μl of DCFH-DA from the 5 mM working solution was added to the tubes to a 100-μM final concentration. The samples were sonicated for 1 min to let the dye permeate the cell wall as *L. incisa* has a thick cell wall, not easily permeable to dyes. Then, samples were incubated at 25°C in the dark for 90 min with gentle shaking using a rocking shaker. After incubation, the cells were washed twice with their respective media by centrifuging at 1500 × *g* for 5 min and suspended in 100-μl of their respective fresh media (for control samples and N-starved cells). Next, 100-μl samples were loaded into 96-well plates, and fluorescence of DCF was measured at a 530-nm emission and 495 excitation wavelength in a Cary Eclipse Fluorescence Spectrophotometer (Varian, United States). Autofluorescence at 680 nm was used to normalize samples. Similarly, additional samples of algal cells with BG-11 (control) and −N mBG-11 without dye were prepared for background correction, and fluorescence was measured. The ROS content was calculated as the change in fluorescence = $[(A_{530}\text{-}A_{680})_{\text{algae +media +dye}} - (A_{530}\text{-}A_{680})_{\text{algae +media}}]$. Aliquots of each sample were also observed under the Zeiss Axio Imager A2 fluorescence microscope (Carl Zeiss AG, Göttingen, Germany) equipped with differential interference contrast (DIC) Nomarski optics under × 1000 magnification, and an AxioCam MRs digital camera, for imaging of ROS generation in the cells.

Volatile Compound Extraction, Identification, and Quantification

Volatile compounds were extracted at the indicated time points from both the *L. incisa* algal biomass and the culture medium. For sample collection, algal samples (10 ml) were harvested by centrifugation at 1800 × *g* for 5 min in falcon tubes. The medium samples were collected in oak-ridge tubes, and algal pellets were transferred to 2-ml safe-lock Eppendorf tubes by adding a minimum amount of the medium. Algal samples were again centrifuged (at 1800 × *g*, 2 min), and the medium samples were added to the respective oak-ridge tubes. Algal and medium samples were processed separately for the extraction of volatiles. For algal biomass and medium samples, 50 μl of internal standard (10 ppm) isobutylbenzene (IBB, Sigma-Aldrich, Israel), 150 μl of hexane and 10–12 glass beads (2.7 mm diameter) were added to the tubes. The tubes were vortexed, sonicated in an ultrasonicator (Branson) for 2 min, and homogenized in a Mini-Beadbeater-24 (BioSpec) in four sequential pulses of 30 s each, with intermediate cooling for 1 min. This procedure did not disrupt the *L. incisa* cells, due to their strong walls. Hexane (100 μl) was again added to the tubes, followed by vortexing and centrifugation at 11,300 × *g* for 10 min at 25°C. Aliquots of hexane fractions (100 μl) were collected and transferred to glass inserts, placed in gas chromatography (GC) vials, flushed with nitrogen gas, and stored at −80°C until analyses. For the medium samples, 1 ml of internal standard (IBB) and 10 ml of hexane were added to the oak-ridge tube containing 10 ml of the medium. The tubes were vortexed for 1 min and centrifuged at 1800 × *g* for 5 min. The hexane layer was collected in glass vials, evaporated under nitrogen to 100 μl, transferred to inserts, placed in GC vials, and stored at −80°C until analyses. For the medium blank, volatiles were extracted from blank mBG-11 and N-free-mBG11 in which no alga was cultivated, as described above for medium controls. For VOC analysis, 1 μl of algal and medium solvent extracts were injected into a TRACE GC Ultra equipped with an Rtx-5SIL mass spectrometer fused-silica capillary column (0.25 μm × 30 m × 0.25 mm, Restek) and a TRACE DSQII quadruple mass spectrometer (Thermo Finnigan). Helium was used as the carrier gas at a flow rate of 1 ml/min. The injector temperature was set to 220°C (splitless mode), the interface temperature was set to 240°C, and the ion source was adjusted to 200°C. The analysis was performed under the following temperature program: 2 min of isothermal heating at 40°C followed by a 7°C min^{-1} oven temperature ramp to 250°C, and then 2 min of isothermal heating. Mass spectra were recorded at 5.23 scan/s with a scanning range of a 40–400 mass-to-charge ratio and an electron energy of 70 eV. Compounds were tentatively identified (>95% match) based on the NIST/EPA/NIH Mass Spectral Library data version NIST 14 (software version 2.0f) using the MassHunter Work Station Unknowns Analysis software B.07.00 (Agilent). Retention index (RI) were also confirmed with RI libraries from the literature (Goodner, 2008; Babushok et al., 2011; Zuo et al., 2012b; de Alencar et al., 2017; Hosoglu, 2018) and online databases such as Flavornet[1], The Pherobase[2] and PubChem[3]. For the medium samples, the chromatogram of the blank medium control was subtracted from each sample and then integrated for compound identification.

Statistical Analyses

A one-way analysis of variance (ANOVA), followed by Tukey's honest significance (HSD) test, was performed for determining the significant differences ($p < 0.05$) between the control and N-starved samples, by separately comparing treatment and time as main factors, using the JMP version 14 software package (SAS Institute Inc., Cary, NC, United States). Additionally, a pairwise

[1]http://www.flavornet.org/

[2]http://www.pherobase.com/

[3]https://pubchem.ncbi.nlm.nih.gov/

t-test was performed to compare the significant differences between the control and N-starved samples at any particular time using JMP. Then, a two-way ANOVA was performed to determine the distinct treatment- and time-dependent responses in *L. incisa* under N-starvation ($p < 0.05$), using Origin Pro 8.5. Furthermore, the volatile datasets (algal and media sets) were log-transformed and auto-scaled (mean-centered and divided by the standard deviation of each variable) in order to give all variables equal weight, regardless of their absolute value. This data pre-processing was helpful in performing a meaningful multivariate analysis, as the detected volatile compound levels were of different orders of magnitude. After pre-processing, a principal component analysis (PCA) and heatmaps with hierarchical clustering (based on the Pearson correlation and average linkage) were performed, using a web-based software, MetaboAnalyst v 4.0[4] (Chong et al., 2019). The PCA plot was used to detect intrinsic clusters and outliers within the dataset, while heatmaps with clustering were generated to assess the relative levels of different volatiles. These analyses were used to identify the discriminant volatiles produced in *L. incisa* and those released in the media during N-starvation.

RESULTS

Culture Growth Assessment

The growth parameters of the N-replete (control) and N-starved cultures were monitored by measuring photosynthetic pigments and biomass production during the course of the experiment. While the Chl (volumetric) content ($\mu g\ mL^{-1}$) increased in the control culture to over 150 $\mu g\ mL^{-1}$ within 6 days, during N-starvation, it significantly declined on the background of the retention of total Car content, resulting in a decrease in the Chl/Car ratio (**Figures 1A,C,E**), in accordance with the previous studies (Solovchenko et al., 2010; Pal-Nath et al., 2017). This decline in Chl was quite pronounced after 3 days of N-starvation, reaching a maximum decline of ca. 9-fold compared with the initial value on day 14 ($p < 0.05$), indicating severe chlorophyll degradation in the N-starved cells (**Figure 1A**). Similarly, the Chl biomass (DW) content (**Figure 1B**) showed a gradual 1.5- to 5-fold decrease under N-starvation. In contrast to the Car volumetric concentration, the levels of Car ($\mu g\ mg^{-1}$ DW) declined less, by 1.2- to 2.2-fold under N-starvation, than the control (**Figure 1D**).

Biomass production decreased under N-starvation compared to the N-replete control culture, reaching 2.54 mg mL^{-1} DW on day 14, as is typical of N-starved *L. incisa* (WT) cultures in agreement with the decline in Chl content. The control cultures demonstrated significantly higher ($p < 0.05$) biomass production during cultivation, reaching 6.38 mg mL^{-1} DW on day 14 (**Figure 1F**). Furthermore, the two-way ANOVA also confirmed considerable treatment-dependent (N-starvation) and significant time-dependent interactions ($p < 0.05$) in the responses of Chl, total Car, and biomass accumulation under N-starvation conditions, except for the Car culture content, which did not show significant time-dependent changes under N-starvation (**Supplementary Table S1**). This also led to an insignificant interaction effect of treatment and time on the Chl/Car ratio ($p < 0.05$) under N-starvation.

Total Fatty Acid (TFA) Production and Alteration in the Fatty Acid Composition

It is established that the total fatty acid (TFA) content (% DW) increases during N-starvation in microalgae, concomitant with the build-up of lipid-enriched biomass and alterations in FA profiles. *L. incisa* showed significant treatment- and time-dependent accumulation of TFA (% DW) under N-starvation as was apparent from the two-way ANOVA ($p < 0.05$; **Supplementary Table S1**), reaching 26.1 $\mu g\ mg^{-1}$ DW on day 14 (1.5-fold higher as compared to the control) under the experimental conditions of this work (**Figure 2A**). Arachidonic acid (ARA) accumulation under N-starvation is a distinctive and biotechnologically important feature of *L. incisa* (Bigogno et al., 2002; Khozin-Goldberg et al., 2016). ARA reached 42.2% of TFA on day 14 as compared to 15.4% of TFA at the onset of the experiment (day 0) (**Figure 2E**). The other alterations in FA compositions (**Figures 2B–E**) were in line with previous studies (Pal-Nath et al., 2017; Kugler et al., 2019). For instance, concurrent with the increase in ARA, there was a characteristic decrease in the C18-PUFAs, linoleic acid (C18:2, *n*6; LA) by 1.4- to 1.8-fold and α-linolenic acid (C18:3, *n*3; ALA) by 1.4- to 7.3-fold ($p < 0.05$) under N-starvation. Oleic acid (C18:1, *n*9; OA) and linoleic acid (C18:2, *n*6; LA) are precursors of ARA and components of TAG, along with ARA, and are channeled upstream of the TAG assembly (Bigogno et al., 2002). Saturated fatty acids (SFAs) decreased mainly due to the decrease in palmitic acid (C16:0, 1.02- to 1.3-fold), while monounsaturated fatty acids (MUFAs) increased mainly due to the increase in oleic acid (C18:1 *n*9; 1.3- to 2.8-fold) as compared to the control ($p < 0.05$). Additionally, the FA profile of control cultures on day 14 was characteristic of that of the late stationary phase with increased proportions of ARA (2.4-fold) and OA (1.5-fold) at the expense of C18 PUFAs (1.6-fold), palmitic (1.4-fold), and palmitoleic acid (C16:1, *n*7, 2.5-fold).

N-Starvation Induces Increased ROS Levels in *L. incisa*

The significant treatment- and time-dependent interaction effects on ROS production were found under N-starvation conditions. N-starved cultures displayed higher ROS levels (>2-fold) as compared to the control (**Figure 3**) during the study period. Although the ROS levels (DCF-FU mg^{-1} DW) were significantly higher in the N-starved cells, a similar pattern of ROS production was determined in both the control and N-starved algae, seemingly related to different biomass productivity levels. Two large peaks of ROS on day 1 (maximal production) and a small peak on day 6 were documented (**Figure 3IA**). The increase in ROS levels in the control nutrient-replete cultures on day 1 may have been due to the "dilution-effect" at the onset of the experiment, which may cause some stress to cells. However, ROS levels normalized with Chl were not altered (**Figure 3IB**).

[4]https://www.metaboanalyst.ca

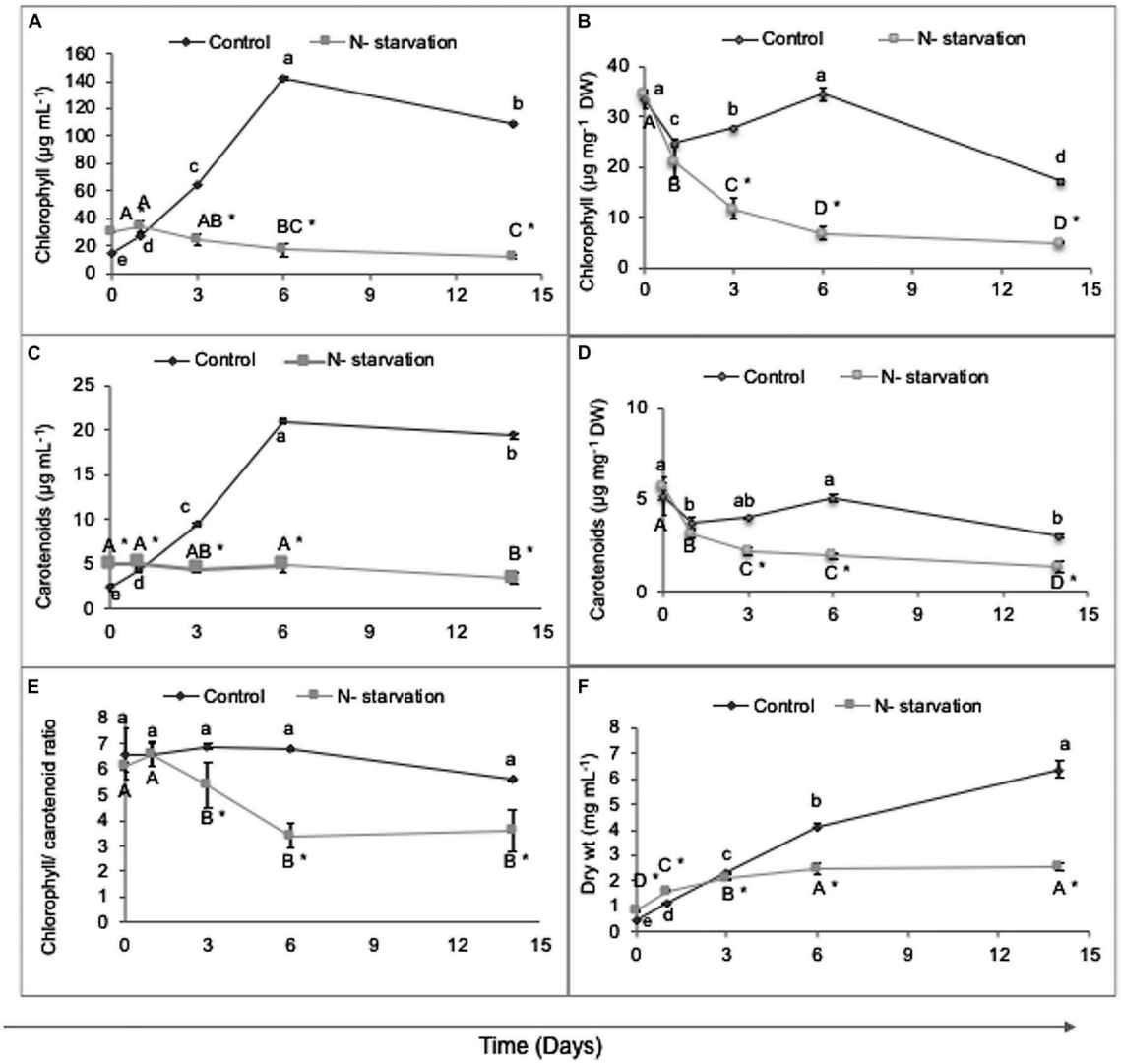

FIGURE 1 | Dynamics of growth parameters under experimental conditions in N-replete (control) and N-starved cultures. **(A)** Chlorophyll volumetric content (µg mL^{-1}), **(B)** chlorophyll content normalized on DW (µg mg^{-1}), **(C)** total carotenoid volumetric content (µg mL^{-1}), **(D)** total carotenoid content normalized on DW (µg mg^{-1}), **(E)** chlorophyll/carotenoid ratio, and **(F)** dry weight content. Data are shown as the mean ± SD of three independent experiments, with two analytical replications. Different letters indicate a significant difference during the course of the experiment within the control (denoted by lowercase) and within the N-starved cultures (uppercase) by one-way ANOVA ($p < 0.05$) followed by Tukey's HSD test. An asterisk indicates a significant difference between the control and the N-starved cultures at any particular time.

The ROS level in the control cultures increased on day 1, again indicating that dilution at inoculation can cause stress; after, it was maintained at lower levels. In N-starved cultures, ROS levels increased rapidly on day 1, peaked on day 3, maintained almost unaltered till day 6, and then declined sharply (**Figure 3IB**). The high ROS levels were maintained till day 6 of N-starvation, simultaneously with the patterns in ARA increase during N-starvation (**Figure 2E**). Imaging of ROS localization in control (**Figures 3IIA–E**) N-starved cells (**Figures 3IIF–J**) was consistent with the pattern of ROS production. The major boost of ROS occurred on day 1 in the cells after the transfer to the N-depleted medium, while only a faint weak fluorescent signal of DCF was visible in the N-starved cells on day 14, mainly in the cytoplasm occupied by lipid droplets. The control cultures on day 14 were in the stationary phase, characterized by nutrient depletion, slow growth, low photosynthetic activity, and a gradual shift to storage lipid formation; these are all consistent with a low level of ROS production.

VOC Profiling

In this work, we investigated the VOC profiles of the *L. incisa* biomass and the culture medium under N-replete (control) and N-starvation conditions to elucidate the patterns of their production and to understand their physiological roles. By using a GC-MS analysis, we detected 42 VOCs from the algal biomass (AVOCs) and 19 from the culture media (MVOCs), which belong

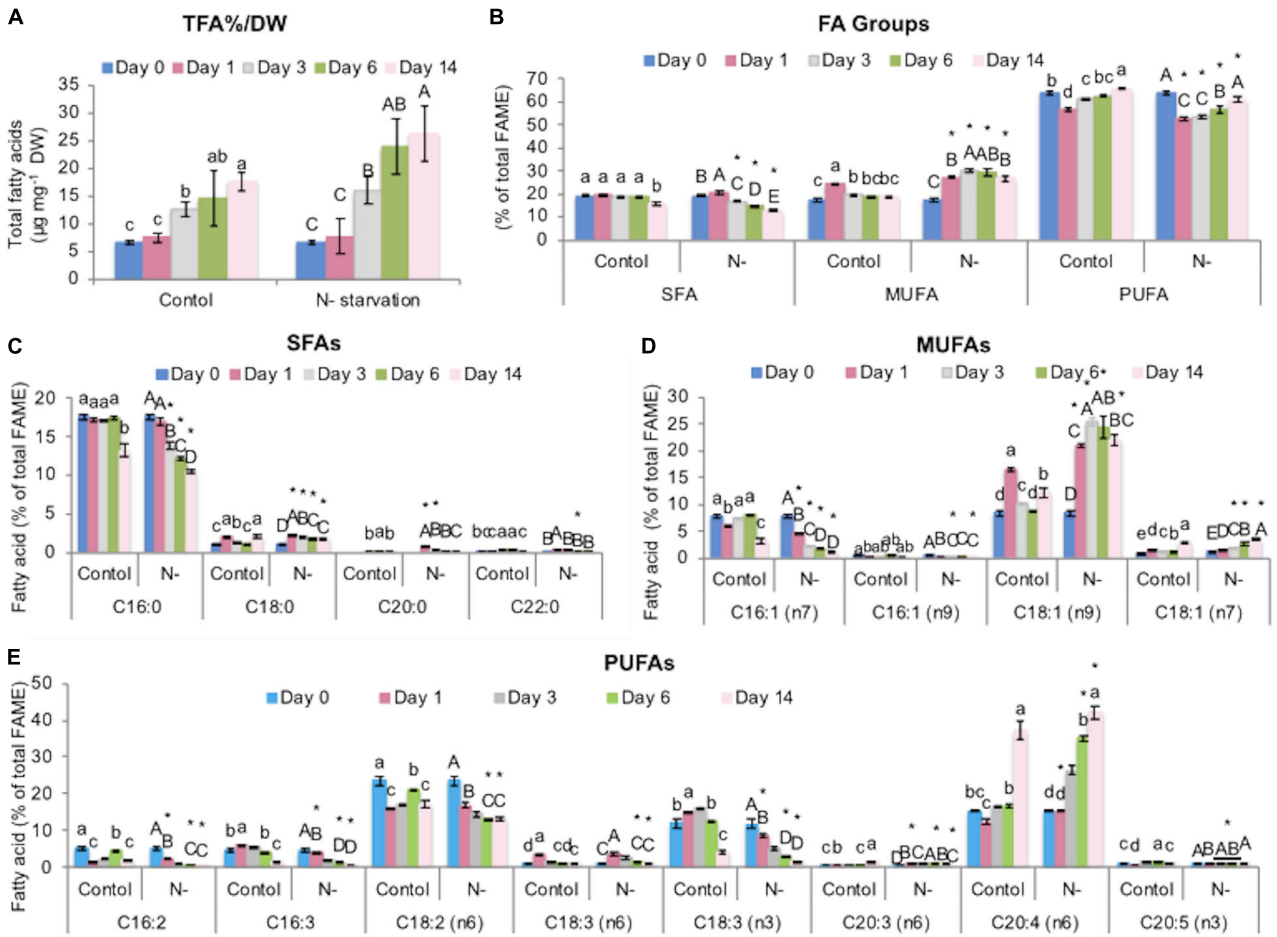

FIGURE 2 | Alterations of fatty acid profiles under experimental conditions in N-replete (control) and N-starved *L. incisa* cultures. **(A)** TFA% DW, **(B)** FA groups, **(C)** SFAs, **(D)** MUFAs, and **(E)** PUFAs. Data are shown as the mean ± SD of three independent experiments, with two analytical replications. Different letters indicate a significant difference during the course of the experiment within the control (denoted by lowercase) and within the N-starved cultures (uppercase) by one-way ANOVA ($p < 0.05$) followed by Tukey's HSD test. An asterisk indicates a significant difference between the control and the N-starved cultures at any particular time determined by a pairwise *t*-test.

to 10 different metabolic classes: alkanes, alkenes, benzenoids, esters, fatty alcohols, fatty aldehydes, fatty acids, ketone, and terpenoids (**Table 1**). The relative contents of the major VOC classes are presented in **Figure 4**, and the detailed contents of all detected VOCs are given in **Supplementary Figures S1–S8**. VOC heat-maps were generated (**Figure 5**) and a PCA was performed (**Figure 6**) to visualize the alterations in the VOC profiles under N-replete and N-starvation conditions and to identify treatment-specific discriminant VOCs (described below in sub-sections).

VOCs Produced by N-Replete *L. incisa*

Characteristic VOC profile of N-replete L. incisa (day 0) control

Among the AVOCs, terpenoids constituted the major class (61.2%) of total AVOCs (TAVOCs), followed by fatty acids (16.8%), alkenes (10.7%), fatty aldehydes (6.5%), and fatty alcohols (3.5%). Alkanes, ketones, and fatty acid esters together represented a minor fraction, 1.4% (**Supplementary Figure S1**). Terpenoids were represented by a monoterpene (α-pinene), a diterpene (*trans*-geranylgeraniol), a diterpene alcohol (phytol), and sequiterpenes (*trans*-beta-ionone, caryophyllene oxide, and neophytadiene), of which phytol accounted for 58.4% of TAVOCs. Among volatile FAs, we detected only few FAs present in the *L. incisa* biomass, such as linoleic acid (LA), which was also the major acyl group in the FAMEs of the control cells, determined by the transmethylation method (**Figure 2**), followed by palmitic, oleic, tetradecanoic, and pentadecanoic acids. Heptadec-8-ene was the major alkene detected, while 1-undecene and 2-pentadecen-4-yne constituted the minor fraction. Remarkably, a series of fatty aldehydes and their respective reduced fatty alcohols were detected, such as 1-undecanal and 1-undecanol; pentadecanal and Z-10-pentadecanol; 9,12-octadecadienal and 9,12-octadecadien-1-ol; 9,12,15-octadecatrienal and 9,12,15-octadecatrien-1-ol; and others. These fatty aldehydes and alcohols are by-products of lipid metabolism and indicate the presence of an active

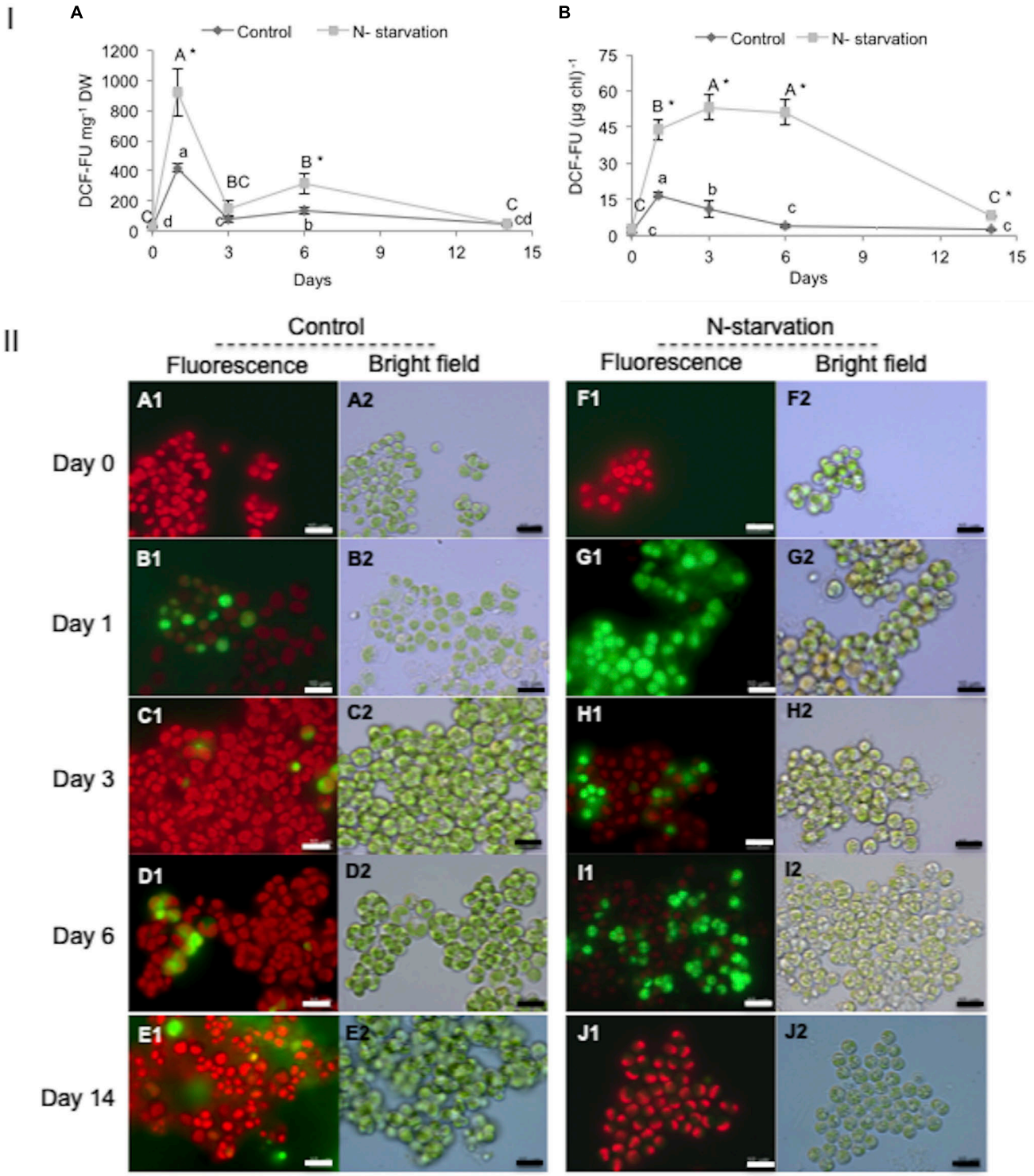

FIGURE 3 | ROS production under experimental conditions in N-replete (control) and N-starved *L. incisa* cultures. **I (A)** ROS levels per dry weight (DCF-FU mg^{-1} DW); **(B)** volumetric ROS levels (DCF-FU Chl^{-1}). Data are shown as the mean ± SD of three independent experiments, with two analytical replications. Different letters indicate a significant difference during the course of the experiment within the control (denoted by lowercase) and within the N-starved cultures (uppercase) by one-way ANOVA ($P < 0.05$) followed by Tukey's HSD test. An asterisk indicates a significant difference between the control and the N-starved cultures at any particular time. **II** Micrographs showing ROS production in control N-replete and N-starved cultures. **II (A1–E1)** Fluorescent micrographs of ROS localization in control cells and **(A2–E2)** their corresponding bright-field images. **(F1–J1)** Fluorescent micrographs of ROS localization in N-starved cultures and **(F2–J2)** their corresponding bright-field images. Scale bar = 10 µm.

TABLE 1 | Volatile organic compounds identified in *Lobosphaera incisa* biomass (AVOCs) and media (MVOCs).

Algal volatile organic compounds (AVOCs)

No.	Compounds	Class	Formulae	Mass	RT* (min)	RI**
1	α-Pinene	Terpenoids (Monoterpene)	$C_{10}H_{16}$	136.2	8.04	951.4
2	Nonane, 5-methyl-	Alkane	$C_{10}H_{22}$	142.28	8.83	980
3	1-Octen-3-one	Ketones	$C_8H_{14}O$	126.199	9.02	996.3
4	1-Octen-3-ol	Fatty alcohol	C_8H1_6O	128.215	9.08	999.7
5	2,3-Octanedione	Alpha-diKetone	$C_8H_{14}O_2$	142.198	9.15	1002.8
6	(E)-oct-2-enal	Fatty aldehyde	$C_8H_{14}O$	126.199	10.57	1067.4
7	1-Undecene	Alkene	$C_{11}H_{22}$	154.29	11.11	1091.32
8	Tetrahydrogeraniol	Fatty alcohol	$C_{10}H_{22}O$	158.2	11.20	1096.1
9	4-Nonenal, (E)-	Fatty aldehyde	$C_9H_{16}O$	140.226	11.59	1113.9
10	Undecane, 5-methyl-	Alkane	$C_{12}H_{26}$	170.34	11.73	1119.5
11	2-Nonen-1-ol, (Z)-	Fatty alcohol	$C_9H_{18}O$	142.24	11.82	1123.03
12	Undecane, 4-methyl-	Alkane	$C_{12}H_{26}$	170.34	11.86	1126.7
13	Undecane, 2,4-dimethyl-	Alkane	$C_{13}H_{28}$	184.36	15.00	1262.6
14	2,4-Decadienal, (E,E)-	Fatty aldehyde	$C_{10}H_{16}O$	152.2	15.84	1304.3
15	1-Undecanal	Fatty aldehyde	$C_{11}H_{22}O$	170.296	15.94	1310.0
16	1-Undecanol	Fatty alcohol	$C_{11}H_{24}O$	172.31	17.56	1393.0
17	*trans*-beta-Ionone	Terpenoids (Sesquiterpenoid)	$C_{13}H_{20}O$	192.3	19.28	1490.54
18	2-Pentadecen-4-yne,(Z)-	Alkene	$C_{15}H_{26}$	206.37	21.05	1591.45
19	Caryophyllene oxide	Terpenoids (Sesquiterpenoid)	$C_{15}H_{24}O$	220.35	21.63	1600.0
20	Heptadec-8-ene	Alkene	$C_{17}H_{34}$	238.4	22.48	1718.00
21	Pentadecanal-	Fatty aldehyde	$C_{15}H_{30}O$	226.4	23.11	1721.0
22	Tetradecanoic acid	Fatty acid	$C_{14}H_{28}O_2$	228.37	23.91	1773.0
23	Z-10-Pentadecen-1-ol	Fatty alcohol	$C_{14}H_{30}O$	214.39	23.99	1777.43
24	Octadecane	Alkane	$C_{18}H_{38}$	254.5	24.32	1801.0
25	Neophytadiene	Terpenoids (Sesquiterpenoid)	$C_{20}H_{38}$	278.5	24.85	1832.5
26	Pentadecanoic acid	Fatty acid	$C_{15}H_{30}O_2$	242.4	25.37	1839.0
27	1-Hexadecanol	Fatty alcohol	$C_{16}H_{34}O$	242.447	25.45	1883.0
28	9,12-Octadecadienal	Fatty aldehyde	$C_{18}H_{32}O$	264.45	25.71	1905.00
29	9,12,15-Octadecatrienal	Fatty aldehyde	$C_{18}H_{30}O$	262.43	25.80	1911.0
30	Octadecanal	Fatty aldehyde	$C_{18}H_{36}O$	268.48	26.14	1935.0
31	9,12-Octadecadien-1-ol, (Z,Z)-	Fatty alcohol	$C18H_{34}O$	266.46	26.47	1960.0
32	9,12,15-Octadecatrien-1-ol, (Z,Z,Z)-	Fatty alcohol	$C_{18}H_{32}O$	264.45	26.56	1968.0
33	n-Hexadecanoic acid	Fatty acid	$C_{16}H_{32}O_2$	356.4	26.90	1996.0
34	Linoleic acid methyl ester	Fatty acid ester	$C_{19}H_{34}O_2$	294.47	27.81	2053.7
35	α-Linolenic acid methyl ester	Fatty acid ester	$C_{19}H_{32}O_2$	292.46	27.87	2059.5
36	Phytol	Terpenoids (Diterpene alcohol)	$C_{20}H_{40}O$	296.53	28.75	2121.1
37	Linoleic acid	Fatty acid	$C_{18}H_{32}O_2$	280.45	29.19	2143.6
38	α-Linolenic acid	Fatty acid	$C_{18}H_{30}O_2$	278.43	29.21	2150.5
39	Oleic Acid	Fatty acid	$C_{18}H_{34}O_2$	282.46	29.41	2165.16
40	Octadecanoic acid	Fatty acid	$C_{18}H_{36}O_2$	284.4	29.51	2177.6
41	*trans*-Geranylgeraniol	Terpenoids (Diterpene)	$C_{20}H_{34}O$	290.49	29.70	2185.68
42	Arachidonic acid	Fatty acid	$C_{20}H_{32}O_2$	304.47	31.34	2293.0

Media volatile compounds (MVOCs)

S. No.	Compounds	Class	Formulae	Mass	RT (min)	RI
1	2-Hexanone, 3,4-epoxy-	Keto-Ether	$C_6H_{10}O_2$	114.14	7.11	909.0
2	Benzene, ethenyl-	Benzenoid	C_8H_8	104.15	7.17	912.9
3	Heptanal	Fatty aldehyde	$C_7H_{14}O$	114.188	7.39	921.5
4	2-Ethyl-1-(2-hydroxypropyl) cyclopropanol	Alcohol	$C_8H_{16}O_2$	144	7.79	939.1
5	5-Methyl-1-hexene-3,4-dione	Ketone	$C_7H_{10}O_2$	126	7.91	946.2
6	Dimethyl oxalate	Ester	$C_4H_6O_4$	118.08	8.29	962.3

(Continued)

TABLE 1 | Continued

Media volatile compounds (MVOCs)						
S. No.	**Compounds**	**Class**	**Formulae**	**Mass**	**RT (min)**	**RI**
7	2-Heptenal, (E)-	Fatty aldehyde	$C_7H_{12}O$	112.17	8.58	977.6
8	Nonane, 5-methyl-	Alkane	$C_{10}H_{22}$	142.28	8.65	980.0
9	1-Decene, 4-methyl-	Alkene	$C_{11}H_{22}$	154.29	9.92	1037.6
10	Limonene (+)-	Monoterpene	$C_{10}H_{16}$	136.238	10.13	1048.7
11	(E)-oct-2-enal	Fatty aldehyde	$C_8H_{14}O$	126.199	10.83	1079.9
12	2-Nonen-1-ol, (E)-	Fatty alcohol		142.24	11.76	1123.0
13	(3Z,5E)-1,3,5-Undecatriene	Alkene	$C_{11}H_{18}$	150.26	13.51	1190.7
14	*trans*,*trans*-2,4-Nonadienal	Fatty aldehyde	$C_9H_{14}O$	138.21	14.80	1253.2
15	2,4-Decadienal, (E,E)-	Fatty aldehyde	$C_{10}H_{16}O$	152.23	15.85	1305.2
16	2-Decen-1-ol	Fatty alcohol	$C_{10}H_{20}O$	156.269	16.36	1330.6
17	1-Undecanol	Fatty alcohol	$C_{11}H_{24}O$	172.31	17.06	1373.2
18	(S)-(-)-Dodec-2-en-4-ol	Fatty alcohol	$C_{11}H_{24}O$	184.32	18.77	1461.6
19	Benzene, 1- decenyl-, (E)-	Benzenoid	$C_{16}H_{24}$	216.36	20.87	1582.7

**RT, retention time; **RI, retention index. The class of all the volatiles in the table were assigned from the PubChem database, and the compounds were identified with the mass spectrum in the NIST library and RI confirmed with the NIST library, PubChem, Flavornet, The Pherobase and literature (Babushok et al., 2011; de Alencar et al., 2017; Goodner, 2008; Hosoglu, 2018; Zuo et al., 2012b).*

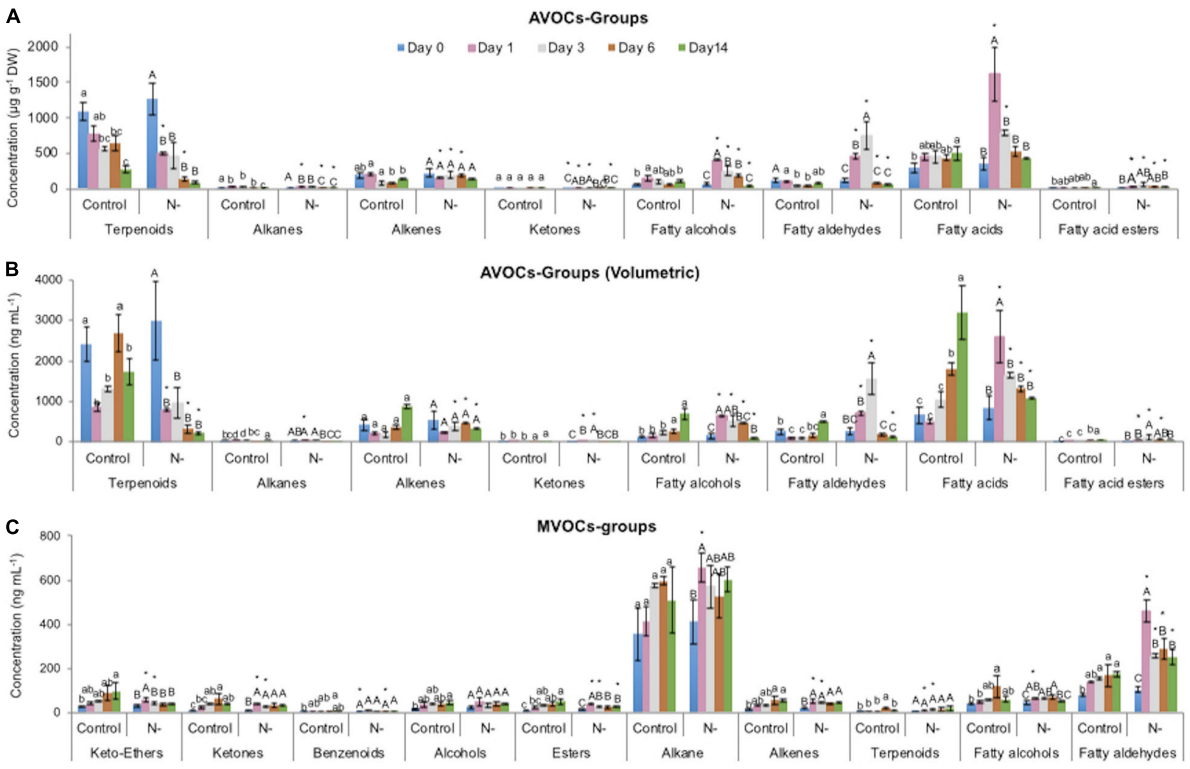

FIGURE 4 | Relative contents of volatile organic compound (VOC) classes identified in *L. incisa* under N-replete (control) and N-starvation conditions. VOCs identified in algal biomass (AVOCs) normalized to DW **(A)**, their volumetric contents **(B)**, and VOCs identified in the culture medium (MVOCs) **(C)**. Data are shown as the mean ± SD of three independent experiments, with two analytical replications. Different letters indicate a significant difference during the course of the experiment within the control (denoted by lowercase) and within the N-starved cultures (uppercase) by one-way ANOVA ($P < 0.05$) followed by Tukey's HSD test. An asterisk indicates a significant difference between the control and the N-starved cultures at any particular time as determined by a pairwise *t*-test.

fatty acyl reductase, mediating the reduction of fatty aldehydes into their respective fatty alcohols. Short-chain fatty alcohols, fatty aldehydes, and ketones were also detected, likely derived from the lipoxygenase (LOX)-mediated oxidative pathway of ARA, of which 1-octen-3-ol and 1-octen-3-one were present in minor amounts, while 2,4-decadienal (*E*,*E*) was present in an

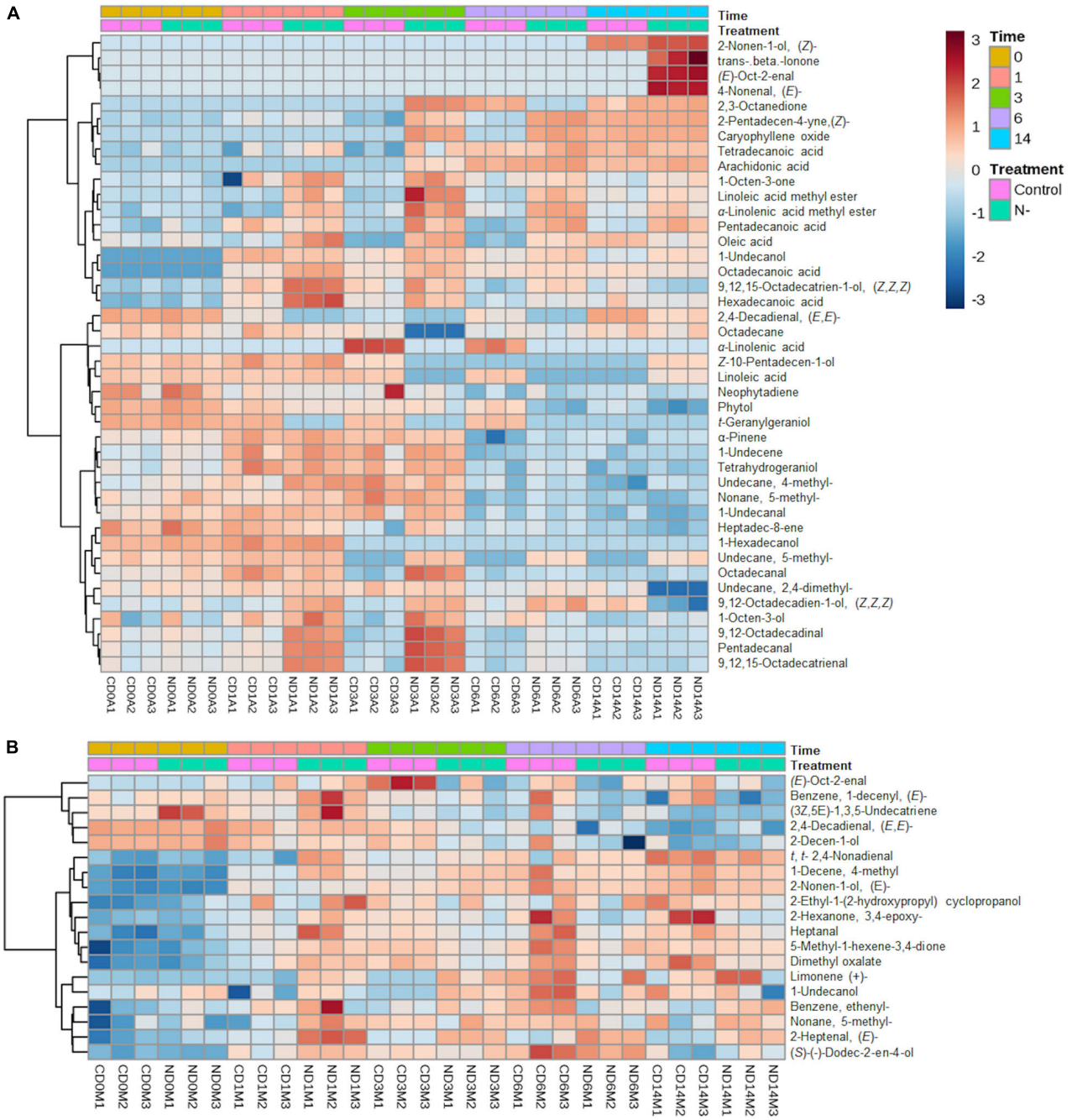

FIGURE 5 | Heat-map of the AVOC profile **(A)** and MVOC profile **(B)** of *L. incisa* cultivated under N-replete (control) and N-starvation conditions, created by hierarchical cluster analysis using Pearson's correlation.

appreciable amount (**Figure 5**). The characteristic AVOC profile of N-replete cells on day 0 thus comprised phytol > heptadec-8-ene > LA, 9,12-octadecadienoic acid > *n*-hexadecanoic acid oleic acid > *trans*-geranylgeraniol > 9,12,15-octadecatrien-1-ol > 9,12,15-octadecatrienal > 9,12-octadecadienal > 9,12-octadecadien-1-ol > 2,4-decadienal(*E*,*E*-).

In contrast to the AVOC profile, alkane was the dominant class (65.2%) of the total MVOCs (TMVOCs) represented by a single compound nonane, 5-methyl, which accounted for only <1% in the AVOCs (**Supplementary Figure S1**). In the TMVOCs, alkane was followed by fatty aldehydes (14.1%), fatty alcohols (6.8%), and keto-ether (4.9%). Terpenoids, which were the major fraction of the AVOCs, constituted a minor fraction in MVOCs. Only 5 out of 19 MVOCs, nonane, 5- methyl-, (E)-oct-2-enal, 2-nonen-1-ol, 1-undecanol and 2,4-decadienal (E,E)-, were present in both the AVOC and MVOC profiles. The characteristic

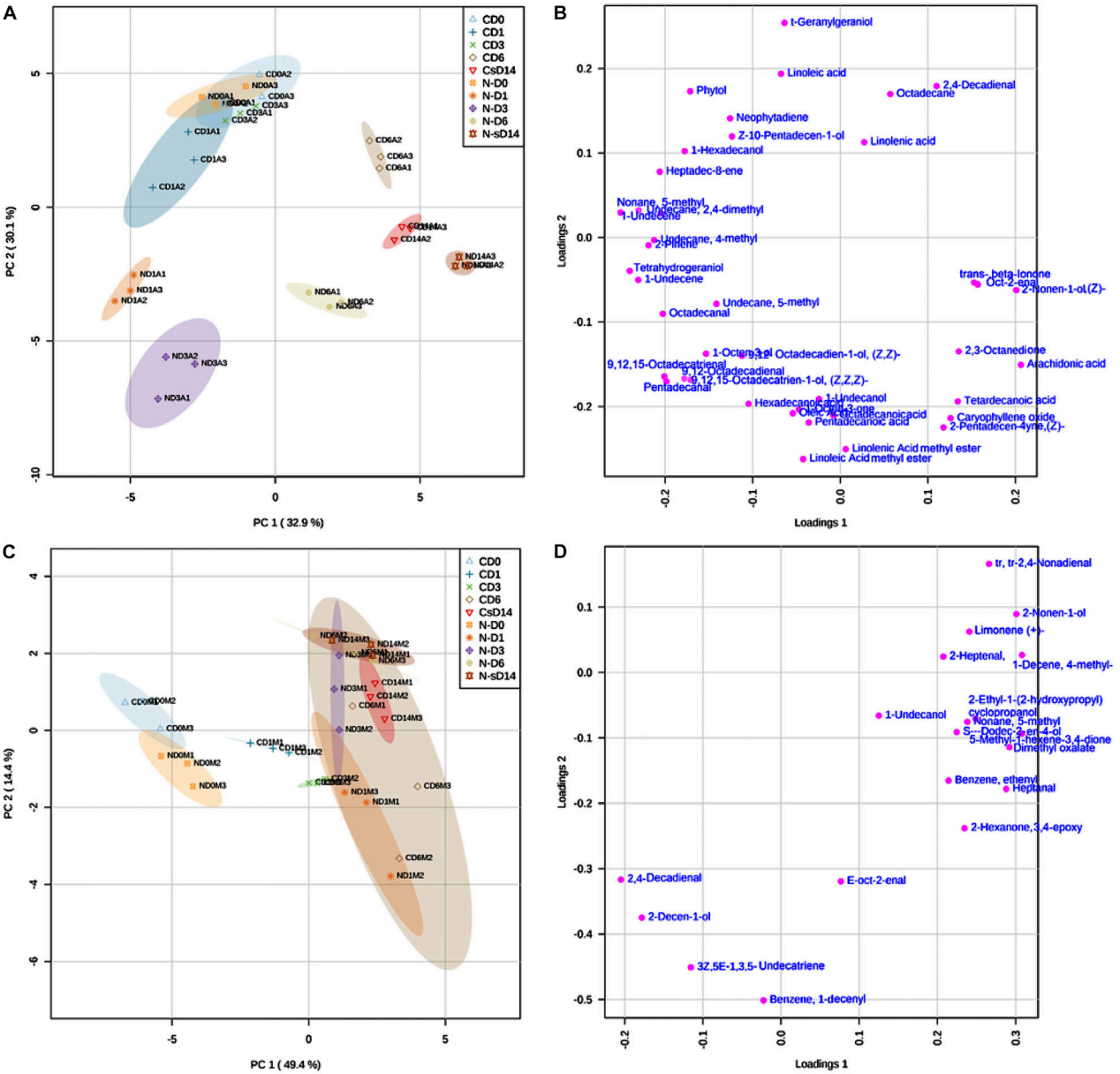

FIGURE 6 | Principal component analyses of the AVOC and MVOC data matrix showing treatment- and time-specific discriminant variables using MetaboAnalyst 4. **(A)** Score plot of the AVOC dataset, **(B)** loading plot of the AVOC dataset, **(C)** score plot of the MVOC dataset, and **(D)** loading plot of the MVOC dataset. Control samples are labeled as CD0, CD1, CD3, CD6, and CD14 for days 0, 1, 3, 6, and 14, respectively. Similarly, N-starved samples are labeled as ND0, ND1, ND3, ND6, and ND14 for days 0, 1, 3, 6, and 14, respectively.

MVOC profile of the control *L. incisa* culture medium comprised nonane, 5-methyl- > *trans*,*trans*-2,4-nonadienal > 2-decen-1-ol > 2-hexanone, 3,4-epoxy > 2-heptenal > 2,4-decadienal (E,E-). Alterations in the VOC profile in the N-replete (control) *L. incisa* culture.

A slight decrease in the volumetric contents of all the AVOCs was detected on day 1, likely in response to culture dilution at inoculation, followed by a constant increase in their production during the experiment, except for terpenoids (**Figures 4**, **5**). However, the AVOC contents, on the DW basis, showed a slight decrease due to the considerably higher increase in the algal biomass. The contents of all the detected MVOCs significantly increased during the cultivation of *L. incisa* under N-replete conditions (**Figure 4**).

Alterations in the VOC Profiles in the Course of N-Starvation

The results showed significant treatment- and time-dependent interaction effects on metabolic alterations in the AVOC and

MVOC profiles under N-starvation ($p < 0.05$) (**Figures 4**, **5** and **Supplementary Table S1**), described by class below.

Terpenoids

Terpenoids that constituted the major fraction of AVOCs detected in the N-replete cells showed significant treatment- and time-dependent decreases (on both a DW and volumetric basis) under N-starvation, mainly due to the continuous decrease in diterpene alcohol and phytol contents as compared to the N-replete control (**Figures 4**, **5**). Other terpenoids detected in the AVOC profile, such as α-pinene and tetrahydrogeraniol, showed only a time-dependent increase in their contents after day 6, while neophytadiene showed insignificant changes. Only in the late stationary phase were *trans*-geranylgeraniol and *trans*-beta-ionone (the later derived from carotenoid degradation) detected, on day 14 (**Supplementary Figure S2**). In contrast to the AVOC terpenoid profile, only one monoterpene, limonene (+)-, was detected in the MVOCs, showing a significant increase in its content under N-starvation as compared to the control, except on day 6 (**Supplementary Figure S8**).

Fatty acids and fatty acid esters

The content of detected volatile fatty acids (on both a DW and volumetric basis) showed significant treatment- and time-dependent increases under N-starvation ($p < 0.05$), as compared to the control culture, with the maximum increase observed on day 1, followed by a gradual decrease in their contents (**Figures 4**, **5**). The increase in volatile FAs detected on day 1 was mainly due to increases in palmitic acid, stearic acid, oleic acid, and LA (**Supplementary Figure S3**), of which only stearic and oleic acids showed an increase in their contents in the biomass analyzed by the transesterification method on day 1. The contents of tetradecanoic and pentadecanoic acids also increased under N-starvation. Here, we note that there were irregularities in the detection of different FA groups, especially of long-chain PUFAs. The latter are generally non-volatile, and indeed, we were able to detect only a few of them without any chemical derivatization; for example, ARA was detected only after day 3, as a minor component.

Further, the contents (DW and volumetric) of two fatty acid esters, LA-methyl ester and ALA-methyl ester that constituted a minor fraction of the N-replete algal AVOC profile, were significantly upregulated under N-starvation, with maximum contents measured on day 3 (4.4- to 15.8-fold higher, compared to the respective controls) (**Supplementary Figure S3**). Their contents then slightly decreased with the duration of N-starvation, suggesting that the formation of volatile C18-FA and C18-FAMEs were compromised in the course of ARA biosynthesis and triacylglycerol formation. In contrast to the AVOCs, no volatile FAs or their esters were detected in the MVOC profile under N-starvation conditions.

Fatty aldehydes and fatty alcohols

Fatty aldehydes in the AVOCs mainly consisted of long-chain unsaturated aldehydes (1-undecanal, pentadecanal, 9,12-octadecadienal, and 9,12,15-octadecatrienal) that showed significant treatment- and time-dependent increases under N-starvation until day 3 (13.0- to 20-fold increase), as compared to control cells. Then their contents decreased (**Figures 4**, **5** and **Supplementary Figure S4**). The short-chain aldehydes, (E)-oct-2-enal, 4-nonenal (E)-, were detected in minor quantities only on day 14 of N-starvation conditions. In addition, 2,4-decadienal (E,E)- was detected mainly in N-replete algal cells, while under N-starvation, it was detected in minor amounts only on day 14. In contrast, fatty aldehydes in the MVOC fraction consisted exclusively of short-chain aldehydes in appreciable amounts, with 2-heptenal (E)- and *trans*,*trans*-2,4-nonadienal being the major VOCs, while heptanal, (E)-oct-2-enal and 2,4-decadienal (E,E)- constituted the minor fraction. This indicated that most of the short-chain fatty aldehydes that are synthesized in algal biomass are released in the medium, suggestive of their possible signaling roles under N-starvation conditions. The contents of the MVOC fatty aldehydes showed significant treatment- and time-dependent increases under N-starvation as compared to the control, however, the maximum increase was observed on day 1 (**Figure 4** and **Supplementary Figure S7**).

Similarly, the contents of fatty alcohols in the AVOCs showed significant treatment- and time-dependent increases under N-starvation conditions, as compared to the control (**Figures 4**, **5**), mainly due to an increase in the relative contents of the long-chain unsaturated C18-fatty alcohols, 9,12,15-octadecatrien-1-ol (Z,Z,Z), 9,12-octadecadien-1-ol (Z,Z) (3.0- to 5.0-fold), and 1-octen-3-ol (1.4- to 2.6-fold). MVOCs contained C9-C12 fatty alcohols that showed a significant increase under N-starvation till day 3 and thereafter decreased (**Figure 4**). No common trend was observed in the relative contents of individual fatty alcohols (**Supplementary Figure S7**).

Ketones

This class comprised only two compounds, 1-octen-3-one and 2,3-octanedione, in the AVOC profile. Both are by-products of lipid metabolism, mainly ARA oxidation. The contents (on both a DW and volumetric basis) of total ketones showed significant treatment- and time-dependent increases under N-starvation ($p < 0.05$), as compared to the N-replete alga, till day 3. They then decreased till day 14, mainly due to relative changes in the content of 1-octen-3-one derived from the ARA-oxidation pathway. Also, 2,3-octanedione was detected in minor amounts only on days 6 and 14 (**Supplementary Figure S5**). Only one ketone compound was detected among the MVOCs, 5-methyl-1-hexene, 3,4-dione of unknown origin and biological function. Its content significantly increased by day 3 ($p < 0.05$) and then decreased as compared to the control, similar to the ketones detected in the AVOC profile of N-starved alga (**Supplementary Figure S8**).

Alkanes and alkenes

The contents (both DW and volumetric) of all the alkanes detected in the AVOCs showed a significant time-dependent increase (1.2- to 2.2-fold) under N-starvation conditions, as compared to control conditions, up to day 3. They then decreased during the experimental period (**Figures 4**, **5** and **Supplementary Figure S6**). The content of total alkenes (**Figure 4**) in the AVOC fraction showed significant treatment- and time-dependent decreases under N-starvation conditions (**Supplementary Table S1**), mainly due to a significant decrease in the contents of

heptadec-8-ene. Among other alkenes detected, no significant change was observed in the content of 1-undecene, while the contents of 2-pentadecen-4-yne, (Z)- significantly increased under N-starvation as compared to N-replete conditions (**Figure 5** and **Supplementary Figure S6**). In the MVOCs, the content of nonane, 5-methyl (alkane) increased under N-starvation conditions as compared to the control, however, its content decreased significantly with time. The content of the alkenes, 1-decene, 4-methyl and (3Z, 5E)-1,3,5-undecatriene, probably the non-enzymatic degradation products of higher alka(e)nes, increased till day 3, followed by a decrease in their contents with the duration of N-starvation conditions as compared to N-replete alga (**Supplementary Figure S8**).

Alcohol, benzenoids, ester, and keto-ether

Volatile organic compounds of these classes were detected only in the MVOC fraction, of which the content of keto-ether (2-hexanone, 3,4-epoxy-) and ester (dimethyl oxalate) showed significant treatment- and time-dependent decreases under N-starvation as compared to the N-replete control. The contents of an alcohol [2-ethyl-1-(2-hydroxypropyl) cyclopropanol] of unknown origin and alkylated benzenoids (benzene, ethenyl- and benzene, decenyl) probably derived from phenylalanine, as other volatile benzenoids that have been previously reported in algae (Santos et al., 2016; Zuo, 2019) did not show any significant changes under N-starvation (**Figure 5** and **Supplementary Figure S8**).

Principle Component Analysis (PCA) of the VOC Profile

The PCA of the AVOC data matrix (PC1: 32.9%, PC2: 30.1%) showed that all biological replicates of each treatment were clustered together, highlighting the reproducibility of the experiment (**Figure 6A**) and assisting in identifying discriminant VOCs for each treatment. All the N-starved AVOC samples were segregated from the control N-replete samples by PC1 (X-axis) except for the N-starved day 0 (ND0) samples that were positioned as expected along with the control samples of days 0 and 3 (CD0, CD1, and CD3) due to their higher loadings of phytol, heptadec-8-ene, LA, *trans*-geranylgeraniol, neophytadiene, and Z-10-pentadecen-1-ol. Also, control AVOCs of day 14 (CD14) were positioned along with the N-starved samples near the PC1 axis, closer to the ND14 samples due to their higher loadings of *trans*-beta-ionone, oct-2-enal and 2-nonen-1-ol that were detected only on day 14 in both control and N-starved algae. The control samples of day 6 (CD6) were separated from other N-replete samples due to their higher ALA contents. The ND1 samples were characterized by higher loadings of 9,12-octadecadien-1-ol (Z,Z)-, 9,12,15-octadecatrien-1-ol (Z,Z,Z)- and 1-octen-3-ol and octadecanal, ND3 by higher loadings of 9,12-octadecadienal, 9,12,15-octadecatrienal, FAs (pentadecanoic, hexadecanoic, octadecanoic), and FA-esters, and ND6 by higher loadings of caryophyllene oxide, 2-pentadecen-4-yne (Z)-, and tetradecanoic acid.

In contrast, the PCA of the MVOCs (PC1: 49.4%, PC2: 14.4%) explained 63.8% of the variance between conditions and showed that CD0 and ND0 MVOC samples are positioned together due to higher loadings of 2,4-decadienal (Z,Z)-, 2-decen-1-ol, 1,3,5-undecatriene and benzene, 1-decenyl (**Figure 6B**). The CD6 formed the largest cluster due to higher variations between their replicates. All the N-starved MVOC samples (ND1, ND3, ND6, ND14), along with CD3 and CD14, formed an overlapping group within the CD6 subset. This is because most of the MVOCs varied only with time and did not show any significant difference between control and N-starvation conditions after day 3 in the course of experiment, except fatty aldehydes, keto-ether, and ester (**Supplementary Table S1**). Within the CD6 cluster, CD14 and ND14 samples were characterized by higher loadings of *trans,trans*-2,4-nonadienal, 2-nonen-1-ol, limonene(+)-, 2-heptenal, and 1-decene, 4- methyl-, pinpointing similar modifications in the MVOC composition in the nutrient-depleted aged culture (CD14) and the N-starved culture (ND14).

Assessment of Putative Genes Involved in VOC Production in *L. incisa*

To reveal the genomic support for the observed patterns of VOC production and composition, we searched the genome and transcriptome of *L. incisa* for genes putatively involved in VOC production. Since many AVOCs that were detected by our analysis, particularly at the earliest time points (day 1), were derived from the chloroplast fatty acids, we analyzed the expression levels of genes that were putatively involved in their generation and release. The transcriptomics data of *L. incisa* were previously generated as described in Siegler et al. (2017) and deposited in the NCBI GEO database under accession number GSE94666.

The increase in the expression of *LiLOX*, encoding the chloroplastic lipoxygenase LOX (g6219) characterized in Djian et al. (2019) was evident 12 h after the transfer to N-starvation, reaching the highest expression level on day 3 (>10-fold). This pattern of expression is consistent with the increase in the contents of C8- and C9- fatty aldehydes, fatty alcohols, and ketones, such as 2-heptenal (*E*)-, 1-octen-3-ol, 1-octen-3-one, and 2-nonen-1-ol, derived from the LOX-mediated oxidation of PUFAs.

The transcript levels of several other genes putatively encoding the chloroplast-localized enzymes involved in the synthesis and modification of fatty acids, such as 3-ketoacyl-ACP reductase (*KAR*), Acyl-ACP thioesterase (*TE*), and long-chain acyl-CoA synthase (*LACS*), were upregulated after 12 h of N-starvation. In *L. incisa*, two putative alcohol-forming fatty acyl reductases are encoded by g12885 and g2791, the latter of which encodes the chloroplastic fatty-ACP reductase (*FAR*), possibly involved in the reduction of acyl-ACPs in the chloroplast. Its transcript levels did not show any significant changes (**Table 2**). Another putative fatty acyl-CoA reductase (*FAR*), g12885, presumably the extraplastidial isoform, showed slightly increasing levels after 12 and 72 h of -N. Further, two out of the three putative phytyl ester synthase (*PES*) genes implicated in phytol metabolism were upregulated after 12 h of N-starvation and decreased below the initial value afterward; this implies that *PES* genes are induced at the early stages of N-starvation, in line with the decreased phytol levels detected in the AVOCs after day 1 in this study.

However, the 12 h time point was not investigated in the present study. Also, the competing pathway of tocopherol biosynthesis from phytol seems to be downregulated, based on a reduction in the expression of the relevant gene (g12840). The genes for lipases g7381 [plastid galactoglycerolipid degradation 1 (*PGD1*)], g14820, and g14821 (galactolipase/phospholipase A1), putatively involved in the release of FAs from chloroplastic glycerolipids (LA and ALA), were all significantly upregulated (2-fold increase after 72 h) under N-starvation (**Table 2**). The transcript abundance of the putative galactolipase/phospholipase A1 genes was higher than *PGD1* in both N-replete and N-starvation conditions. The genome also harbors the genes encoding the putative homologs of ECERIFERUM1 (*CER1*) (g3493), acting in the alkane-forming pathway in higher plants (Bernard et al., 2012) and alkene-forming glucose-methanol-choline (GMC) oxidoreductase (g14991), named fatty acid photodecarboxylase (FAP) in *Chlamydomonas*, involved in the synthesis of long-chain alka(e)nes. *CER1*-like transcripts were upregulated at 12 h and downregulated after 72 h of N-starvation conditions, while GMC oxidoreductase transcripts were only expressed in N-replete conditions and significantly downregulated under N-starvation, in line with the decrease in volatile alkene content under N-starvation in *L. incisa*.

DISCUSSION

N-starvation conditions are known to inhibit growth and chlorophyll content, and to trigger chloroplast degradation and cellular component reorganization in microalgae. Physiological responses of *L. incisa* to N-starvation were observed, such as a decrease in chlorophyll on the background of total carotenoid retention, ROS overproduction, resulting in cellular oxidative stress, and lipid remodeling associated with the ARA-rich TAG biosynthesis in accordance with previous studies (Bigogno et al., 2002; Pal-Nath et al., 2017; Kugler et al., 2019). ROS may act as a stimulus for triggering lipid accumulation under N-starvation (Nagappan et al., 2020) consistent with our findings on the higher ROS levels attained under N-starvation as compared to N-replete cultures. *Lobosphaera incisa* was shown to be extremely sensitive to chemical ROS-inducers applied soon after the transfer to N-starvation, when expression of antioxidant enzyme-encoding genes drastically decreased (Pal-Nath et al., 2017). As we showed here, this corresponds to the early boost of ROS and VOCs. The decrease in ROS levels occurred with time in N-starved cultures, along with the enhancement in LC-PUFA (ARA) accumulation. This may be explained by ARA esterification into TAG and sequestration in lipid droplets, which also accumulate beta-carotene (Solovchenko, 2012; Pal-Nath et al., 2017). The latter may shield ARA-rich TAG from oxidation in the N-starved cells.

In this study, we focused on the dynamics of VOC production to assess the changes in their profile and the physiological roles in *L. incisa* during N-starvation. A wide array of VOCs were detected in *L. incisa*, mainly from terpenoids, FAs, fatty aldehydes, fatty alcohols, ketones, alkanes, alkenes, keto ethers, benzenoids, alcohols, and esters, in line with previous reports in other algae (Zuo et al., 2012b; Durme et al., 2013; Santos et al., 2016; Achyuthan et al., 2017; Zhou et al., 2017; Hosoglu, 2018; Lafarge and Cayot, 2019; Zuo, 2019). However, no sulfur-containing VOCs or 2- keto acids and derivatives derived from branched-chain amino acid pathway were detected in either AVOCs or MVOCs, probably due to the use of ultrasound-assisted VOC extraction in hexane, where the VOCs having low boiling points may have been lost during the extraction procedure. Lafarge and Cayot (2019) also reported the dominance of terpene, FAs, alcohols, aldehydes, and alkanes in the volatile profile of *Chlorella vulgaris* and the absence of sulfur-containing and 2-keto acids in volatile profiles obtained by ultrasound-assisted liquid-liquid extraction with azeotrope propan-2-one/cyclopentane, while these compounds were present when the VOCs were obtained using the SPME method. These authors also suggested that differences in VOCs profiles occurred because the ultrasound-assisted liquid extraction allowed the extraction of VOCs mostly having boiling points $>160^{\circ}$C and a high log P (>3) as compared to the SPME method (Lafarge and Cayot, 2019). It would be interesting in the future to compare the VOC profile using SPME to the data obtained in the present study.

Response to N-starvation is a complex process, involving multiple mechanisms and cell responses, which dynamically progress with the duration and severity of the stress, spanning the enhanced nitrogenous compounds scavenging and repurposing after the transfer to N-deprived medium followed by catabolic degradation of proteins and nucleic acids (Kokabi et al., 2019). Such conditions can generate a broad array of molecules including reactive nitrogen species (RNS), among others. The results showed increases in VOCs (both in the biomass and those released in the medium) under N-starvation as compared to the N-replete conditions, similar to the pattern of the DCFDA-detected radical generation. Given a strong decrease in the abundance of anti-oxidant metabolites (e.g., glutathione forms) under N starvation conditions along with a gradual increase in MDA documented in our previous studies (Pal-Nath et al., 2017; Kokabi et al., 2019), we assumed that the majority of DCFDA-detected species were ROS. However, considering limitations of the DCFDA assay in differentiating between ROS and RNS and considerations noted above, the contribution of RNS can not be ruled out and should be further studied. The highest total VOC emission (AVOCs and MVOCs) on day 1 corresponded to the peak of ROS, and showed a gradual decrease with time. The major AVOCs and MVOCs that increased were volatile free fatty acids, fatty aldehydes, fatty alcohols, ketones, and fatty acid esters derived from oxidative lipid metabolism (enzymatically or non-enzymatically via ROS-mediated mechanisms). These oxygenated VOCs were suggested to act as ROS scavengers in microalgal cells, thereby lowering the oxidative damage under N-starvation (Zuo, 2019). Our data corroborate that the release of a fraction of chloroplast-lipid-derived unesterified FAs and generation of their oxygenated VOC products constitute the fast response of the *L. incisa* cells to N-shortage before the major changes in the physiological parameters and storage lipid accumulation become apparent. Interestingly, this triggered the production of the homologous series of VOCs (fatty aldehydes, fatty alcohols) derived predominantly from the chloroplast C18

TABLE 2 | Putative genes involved in VOC biosynthesis in *L. incisa* and their expression after 12 and 72 h of N-starvation conditions based on transcriptomics analysis.

Gene_ID	Description	Transcription (FPKM)		
		Time 0	N-12 h	N-72 h
g6219	Lipoxygenase (LiLOX)	208.6	422.9	1643.4*
g11127	3-ketoacyl-ACP reductase (KAR)	76.5	339.2*	153.3*
g22	Acyl-ACP thioesterase	35.2	144.5*	145.5*
g3508	Long-chain Acyl-CoA synthase (LACS)	10.9	13.1	12.8
g2791	Fatty-ACP reductase (FAR)	10.5	7.8	7.8
g2611	Phytyl ester synthase (PES)	6.1	6.8	2.9*
g11590	Phytyl ester synthase (PES)	2.3	14.5*	2.2
g1850	Phytyl ester synthase (PES)	7.2	12.7*	1.7
g12840	vitamin E biosynthetic process from phytol	20.3	9.7*	10.4
g14820	putative galactolipase/phospholipase A1	529.4	560.3	1147.1*
g14821	putative galactolipase/phospholipase A1	344.8	179.7	1074.3*
g14991	glucose-methanol-choline oxidoreductase hydrocarbon forming from fatty acids	154.8	6.4*	0.3*
g7381	plastid galactoglycerolipid degradation1	9.0	13.1	27.6*
g5103	TAG lipase	1.7	1.8	35.1*
g2330	Long-chain enoyl-CoA-like reductase	79.8	83.9	110.4
g3493	Long-chain enoyl-CoA reductase-like	15.7	29.7	8.8
g13347	Wax synthase (MBOAT2 protein with WAX synthase domain)	29.1	47.9	40.7
g8197	Wax synthase (MBOAT2 protein with WAX synthase domain)	18.6	26.5	16.0
g12885	Fatty acyl-CoA reductase (FAR)	19.3	25.9*	18.6*
g7129	Lipase/lipoxygenase putative	18.3	121.1*	128.0*
g4221	Aldehyde dehydrogenase (ALDH)	34.4	28.5	19.4

*The significance of change is indicated by * (p value at a false discovery rate of 0.05). FPKM: Fragments Per Kilobase Million. Conditions and methods of the transcriptomics analysis are described in Siegler et al. (2017). Time 0: nutrient-replete culture; 12 and 72 h of N starvation under 150 μmol photons m^{-2} s^{-1}. Predicted chloroplast localization is indicated by light green color.*

PUFA (LA and ALA), which are FA components of the major chloroplast glycerolipids. This was associated with the highest ROS levels detected on day 1, the upregulation of genes putatively involved in FA biosynthesis and modification (such as *KAR*, *acyl ACP thioesterase*), and VOC formation (such as *LiLOX*, *thioesterase*, *FAR*), which began only at 12 h of N-starvation and maintained higher transcript levels until day 3 (**Table 2**). In addition, after prolonged N-starvation, when the ALA pool in the chloroplast lipids decreased and other *de novo* synthesized FAs and ARA became the predominant FAs and were sequestered in lipid droplets (Solovchenko, 2012; Pal-Nath et al., 2017; Kugler et al., 2019) ROS and VOCs decreased (**Figures 2–4**). This indicated that FA channeling toward TAG-enriched lipid droplet formation is a relatively late response, as compared to VOC generation, and that VOCs may act as early signals triggering the cell response for the genetic and metabolic changes required for initiating ARA accumulation. Alternatively, it may also be possible that unsaturated chloroplast FAs are removed from chloroplast lipids and redirected toward TAG assembly at this early stage under N-starvation. The excess FAs may be oxidized to produce VOCs that could serve the multiple functions of ROS scavengers and signaling molecules; in addition, they could also be oxidized for energy. However, the probability of the alternative pathway is less plausible since the genes encoding chloroplastic lipases implicated in the recycling of chloroplastic acyl groups for TAG formation, *PGD1* (g7381) and *galactolipase/phospholipase A1* (g14820 and g14821), were significantly upregulated only after 3 days, indicating that the channeling of chloroplast FAs toward TAG lags behind VOC generation. *PGD1* was shown to be the main lipase acting on the specific molecular species of the major chloroplast galactolipid MGDG in *Chlamydomonas reinhardtii* and is important for TAG accumulation (Du et al., 2018). However, in *L. incisa*, its transcript abundance was lower than other putative chloroplastic lipases (**Table 2**). In addition, g12885 encoding another putative non-chloroplastic lipase/lipoxygenase was upregulated at 12 h and maintained a higher transcript level till day 3; it may be involved in FA oxidative metabolism along with *LiLOX*.

There are a few reports indicating increased VOC (aldehydes, alcohols, ketones, esters, monoterpenes) production in *Chlamydomonas reinhardtii* under acetic acid, NaCl, and Na_2CO_3 stresses Zuo et al. (2012a, 2015) where VOCs were speculated to be involved in adjusting ROS levels and inducing defense responses. Zuo et al. (2012b, 2015) showed that stress-induced VOCs act as information agents and transfer messages to other cells to prepare them for the upcoming stress. They showed that VOCs released by *C. reinhardtii* undergoing programmed cell death (PCD), under NaCl and Na_2CO_3, stresses, can transfer chemical messages to healthy *C. reinhardtii* cells, affecting their normal growth and antioxidant responses Zuo et al. (2012b, 2015). The function of VOCs as signal molecules thus seems to be emerged in the primitive photosynthetic green microalgae, and retained in higher plants (Kessler et al., 2006; Ameye et al., 2018).

Furthermore, the increased fatty aldehydes and fatty alcohols under N-starvation were particularly dominated by long-chain fatty aldehydes and their corresponding alcohols [9,12-octadecadienal, 9,12,15-octadecatrienal, 9,12-octadecadien-1-ol, (*Z*,*Z*,*Z*-), and 9,12,15-octadecatrien-1-ol, (*Z*,*Z*,*Z*-)] in AVOCS, but by short-chain aldehydes and alcohols in MVOCs (heptanal, (E)-oct-2-enal, *trans*,*trans*-2,4-nonadienal, 2,4-decadienal, 2-decen-1-ol, and *S*-(-)-dodecen-4-ol). Long-chain fatty aldehydes and fatty alcohols may be synthesized in *L. incisa* by the fatty acyl-CoA/ACP reductase-dependent pathway established in plants and microorganisms (Rowland and Domergue, 2012; Zheng et al., 2012; Liu et al., 2014; **Figure 7**). First, fatty acyl-ACPs from *de novo* FA biosynthesis are converted to free fatty acids (FFAs) and fatty acyl-coenzyme A (CoA) in reactions sequentially catalyzed by acyl-ACP thioesterase (g22) and LACS (g3508). Next, fatty acyl-CoAs can be reduced to fatty aldehydes or fatty alcohols by fatty acyl-CoA/ACP reductases (*FAR*; g2791, g12885) in a NADPH-dependent reaction, which are further converted to fatty alcohols by an unknown alcohol dehydrogenase or aldehyde reductase (**Figure 7**). Alternatively, fatty acyl-CoA can be directly converted to fatty alcohols by FAR consuming four NADPH molecules. The reason for this preference is not known. Fatty acyl-CoA/ACP reductases have been reported in various organisms (Rowland and Domergue, 2012; Zheng et al., 2012; Liu et al., 2014). Both aldehyde- and alcohol-generating FARs have been purified from pea leaves (Vioque and Kolattukudy, 1997) while in algae, only aldehyde-generating FAR has been reported from *Botryococcus braunii* (Wang and Kolattukudy, 1995) showing homology with bacterial FAR. FARs are categorized into two groups, fatty acyl-CoA reductase and fatty acyl-ACP reductase, depending on their substrate preferences for fatty acyl-CoA and fatty acyl-ACP, respectively, and localization. *L. incisa* seems to harbor harbors both types of FAR, and based on the higher transcript abundance, it seems that fatty acyl-CoA reductase is the key enzyme in fatty aldehyde/alcohol synthesis, and is significantly upregulated, along with thioesterase, under N-starvation (**Table 2**).

The short-chain aldehydes and alcohols are degradation products of the oxidative metabolism of either C18 (LA or ALA) or C20 PUFAs (ARA), generated either by the enzymatic action of lipoxygenase (LOX) and hydroperoxide lyase (HPL) (**Figure 8**) or via non-enzymatic degradation (**Figure 9**) caused by enhanced ROS levels under N-starvation. Recently, a lipoxygenase has been characterized in *L. incisa* (*LiLOX*) (Djian et al., 2019) that exhibited a linole(n)ate13S-LOX and an arachidonate 15S-LOX specificity but showed maximum activity with ALA. LOX oxidizes PUFAs to their corresponding hydroperoxides that, after the action of hydroperoxide lyase (HPL), lead to the formation of short-chain unsaturated fatty aldehydes and fatty alcohols (Andreou and Feussner, 2009; Kumari, 2017). In the case of *LiLOX*, all the major LOX products detected in Djian et al. (2019) lead to the formation of hexa(e)nal, which was not detected in our study. It was possibly lost during extraction as we performed liquid-liquid extraction and not solid-phase microextraction (SPME) for VOC analyses. However, the upregulation of *LiLOX* transcripts (**Table 2**) under N-starvation, together with the presence and increased contents of other short-chain aldehydes and alcohols detected in our study, such as 2-heptenal (E)-, 1-octen-3-ol, and 2-nonen-1-ol, indicated the upregulation of other N-starvation-induced LOX positional isomers, such as 12-hydroperoxyoctadecatrienoic acid (12-HpODE) derived from ALA oxidation and 12-hydroperoxyeicosatetraenoic acids (12-HpETE) derived from ARA oxidation (**Figure 8**). The 2,4-decadienal, detected in low amounts in both the AVOCs and MVOCs of N-replete and N-starved algae, was likely derived from the LOX-HPL-mediated oxidation of ARA via 11-HpETE (Akakabe et al., 2003; Boonprab et al., 2019; **Figure 8**). LiLOX has a strong preference for the tail-first orientation, but it loses its preference if the FFA substrate is protonated or the pH of the reaction medium is lowered, leading to the entrance of substrates from a head-first orientation and the formation of other positional isomers (Djian et al., 2019). The positional and regiospecificity of LOX products and the induction of additional LOX isoforms under N-starvation need further investigation. Furthermore, LiLOX is a non-heme Fe-enzyme and its interaction with ROS may be also a source for radical generation (Kalyanaraman et al., 2012). During LOX reaction, when PUFA substrate enters the active site of LOX, the *bis*-allylic carbon localizes itself next to the Fe^{3+} of the LOX. The non-heme iron abstracts one of the two hydrogen atom on the *bis*-allylic carbon, and get reduced Fe^{2+} generating a free radical on the acyl chain. Free radical is delocalized over the acyl carbon which undergoes rearrangement and activates dioxygen molecule forming a peroxyl radical on the acyl chain followed by reduction of peroxyl radical and oxidation of Fe back to its oxidized Fe^{3+} state (Djian et al., 2019). However, the plausibility of the ROS-mediated non-enzymatic oxidation of PUFAs cannot be overlooked (due to high ROS levels), which may lead to the formation of other fatty aldehydes and alcohols (*trans*,*trans*-2,4-nonadienal, 4-nonenal, oct-2-enal and 2-decen-1-ol) derived from non-enzymatic PUFA oxidation (**Figure 9**). These short-chain unsaturated aldehydes and alcohols have proven roles as signaling molecules in inducing defenses against wounding,

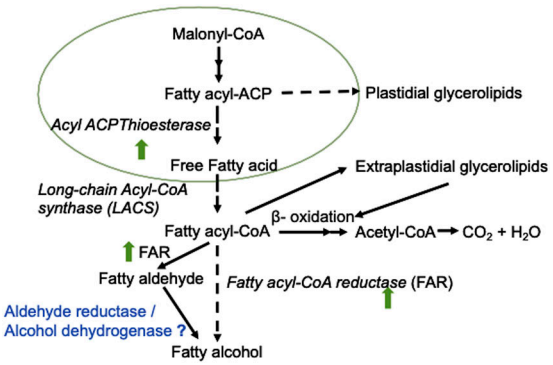

FIGURE 7 | A summary scheme of the suggested biosynthetic pathway of long-chain fatty aldehydes and fatty alcohols in *L. incisa*. The proposed pathway is constructed after the long-chain fatty alcohol biosynthetic pathway reconstructed in *Escherichia coli* (Zheng et al., 2012; Liu et al., 2014). Green upward arrows indicate the upregulation of respective genes in the *L. incisa* transcriptome under N-starvation.

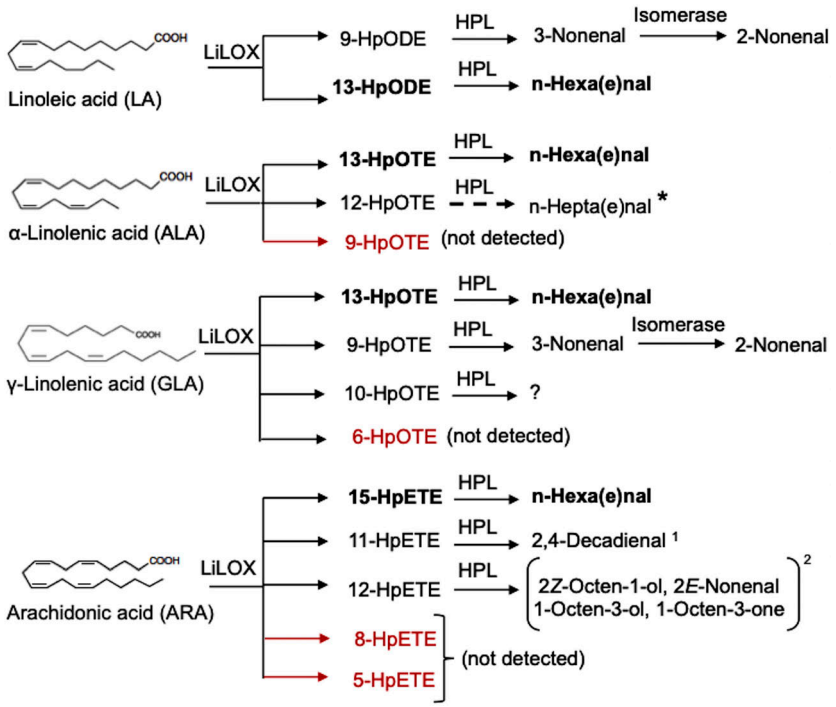

FIGURE 8 | Putative oxidation products of *L. incisa* lipoxygenase (LiLOX) adapted after Djian et al. (2019). Compounds shown in bold font are the major products detected in *L. incisa* and those in red font were not detected (Djian et al., 2019). A hypothetical pathway indicated by dashed arrow. [1]: modified after Akakabe et al. (2003) and Boonprab et al. (2019) as defined for macroalgae, [2]: modified after Kihara et al. (2014) and Chen et al. (2019), defined in *Marchantia polymorpha* and *Pyropia haitanensis,* respectively. HpODE: hydroperoxyoctadecadienoic acid, HpOTE: hydroperoxyoctadecatrienoic acid, HpETE: hydroperoxyeicosatetraenoic acid, HPL: hydroperoxide lyase.

herbivores, and pathogens in algae in the aquatic environment (Wichard et al., 2005; Sabharwal et al., 2017; Chen et al., 2019). The higher contents of these compounds in the MVOCs, as compared to the AVOCs, indicate that they are released in the medium soon after their formation and may be involved in transferring information to other cells in the culture. A similar role can be assigned to nonane, 5- methyl-, which was detected in the highest amount in the MVOCs but accounted for a minor fraction in the AVOCs, however, this proposition needs experimental evidence.

Despite the increase in AVOCs under N-starvation, the degradation of chloroplasts resulted in a decrease in terpenoids, mainly due to the decrease in phytol. Phytol, the prenyl side chain of chlorophyll, is derived from geranylgeraniol by the reduction of three double bonds. The conversion of geranylgeraniol to phytol is linked to chlorophyll synthesis, which is catalyzed by protein complexes associated with the thylakoid membranes (Gutbrod et al., 2019). Chlorophyll degradation releases a large amount of phytol that is either re-incorporated into chlorophyll or utilized for tocopherol (vitamin E), phylloquinol (vitamin K), or fatty acid phytyl ester production (vom Dorp et al., 2015; Gutbrod et al., 2019). However, under N-starvation, in *L. incisa*, phytol does not seem to be utilized in either pathway, as indicated by the downregulation of genes involved in putative phytyl ester synthases (*PES*; g2611, g11590, g1850) and the vitamin E biosynthetic process from phytol (**Table 2**). Since the phytol content decreased in VOCs under N-starvation, it is possible that it was degraded to other autoxidation products as described previously in algae (Rontania and Volkman, 2003) though these compounds were not considered in this study. Among other terpenoids, α-pinene, neophytadiene, *trans*-beta-ionone, and caryophyllene oxide have been reported to increase in plants and algae under environmental perturbations (Meskhidze et al., 2015; Ahn et al., 2016) and thus may serve indicators of excessive stress in *L. incisa*. Furthermore, there was an increase in limonene (+)-, the only monoterpene identified in the MVOCs under N-starvation. It has a proven role in plants in inducing defense responses against herbivory and attracting pollinators. In addition, it may act as a chemical information messenger in *L. incisa*, but this needs further investigation.

Heptadec-8-ene can be synthesized in the green microalgae following the loss of the carbonyl group from oleic acid (**Figure 10**) by a light-dependent pathway in the chloroplast, either catalyzed by FA photodecarboxylase (FAP), a glucose-methanol-choline (GMC)-oxidoreducatse identified in Sorigué et al. (2017), or via the formation of an aldehyde intermediate. Both putative GMC-oxidoreductase and *CER1*-like genes have been identified in *L. incisa*. The former pathway catalyzed by a FAP homolog seems to be the major pathway in *L. incisa* based on the correlation between the content of the detected product and the transcript levels (g14991). Both were apparent in the N-replete cells. FAP has recently been identified

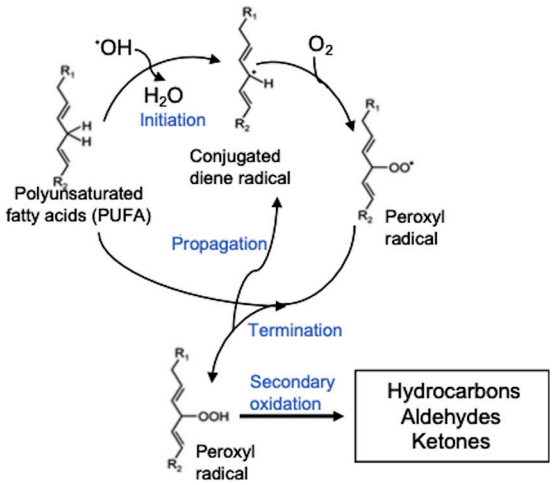

FIGURE 9 | Volatile lipid oxidation products produced via ROS-mediated oxidation of polyunsaturated fatty acids. R1 and R2 are alkyl radicals.

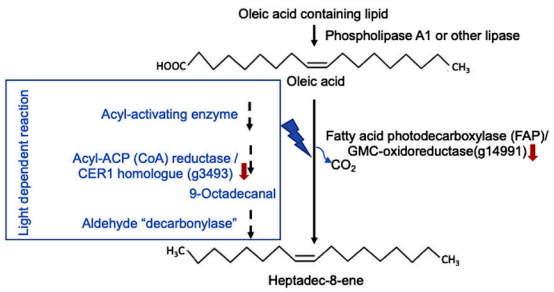

FIGURE 10 | Putative 8-heptadecene biosynthetic pathway in *L. incisa*. Heptadec-8-ene may be synthesized by a light-driven reaction catalyzed by fatty acid photodecarboxylase (FAP), a glucose-methanol-choline (GMC)-oxidoreductase, as described in the related green microalga *Chlorella variabilis* (Trebouxiophyceae) (Sorigué et al., 2017), which may lead to the formation of (n-1) alka(e)ne from fatty acids. Another possibility for heptadec-8-ene formation is via a plant-type light-dependent pathway involving acyl reduction and formal decarbonylation reactions, modified after (Sorigué et al., 2016).

in *Chlorella variabilis* and *C. reinhardtii*, yet 7-heptadecene derived from *cis*-vaccenic acid was the major product. This enzyme was shown to exhibit broad substrate specificity. *CER1*/3 gene homologs of higher plants were not identified in these two green microalgae but were present in the genomes of *Ostreococcus tauri* and *Phaeodactylum tricornutum* (Sorigué et al., 2016). These authors reported a decrease in heptadecene in *C. reinhardtii* after 24 h of transferring to N-starvation. This is in line with the putative *FAP* transcript abundance and VOC data in *L. incisa*. Further characterization of *FAP* (GMC-oxidoreductase) and *CER1* genes would help in elucidating the biochemical role of alka(e)nes and regulating their formation in *L. incisa*. Expanding the repertoire of high-value molecules can aid in realizing *L. incisa*'s biotechnological potential.

Lobosphaera incisa is a potent photosynthetic source of ARA (Bigogno et al., 2002; Khozin-Goldberg et al., 2016). Here, we also explored the possible biotechnological applications of the VOCs, other than FAs, detected in this study by mining the information from available databases and literature. Most of the detected fatty aldehydes and fatty alcohols are ingredients in essential oils and flavoring agents, and are used in the food, cosmetics, and perfume industries (Berger, 2009; Santos et al., 2016). However, the long-chain fatty aldehydes and fatty alcohols that were detected in appreciable amounts under N-starvation conditions can be utilized for these biotechnological applications, such as 9,12-octadecadienal (222.58 $\mu g\ g^{-1}$ DW), 9,12,15-octadecatrienal (325.4 $\mu g\ g^{-1}$ DW), pentadecanal (178.1 $\mu g\ g^{-1}$ DW), 9,12-octadecadien-1-ol (*Z,Z*)- (80 $\mu g\ g^{-1}$ DW), and 9,12,15-octadecatrien-1-ol (*Z,Z,Z*)- (292.4 $\mu g\ g^{-1}$ DW). These VOCs are antioxidants and insect pheromones, and have a multitude of commercial applications as detergents, surfactants, plasticizers, defoamers, and solubility retarders (Zheng et al., 2012). The applications of molecular tools by targeting biosynthetic genes/enzymes (thioesterase, FAR, LOX) can help in obtaining higher yields of these long-chain fatty aldehydes and alcohols, along with other VOCs (including those derived from ARA) of commercial interest, such as 2-heptenal (E)-, 2,4-decadienal, 2,4-nonadienal, and limonene (+)-. Zheng et al. (2012) have optimized the C16/C18-fatty alcohol yields by co-expressing *thioesterase acyl-CoA synthase* and *FAR* genes in engineered *E. coli*. FAP could be another enzyme of important commercial interest for obtaining long-chain alka(e)nes as energy-relevant molecules.

In conclusion, N-starvation stimulates VOC production in the green microalga *L. incisa*. VOCs may play multiple roles, including as ROS scavengers and chemical messengers. VOCs transfer stress signals to other algae in the culture thereby, instigating *L. incisa* cells to remodel their lipid metabolism toward TAG biosynthesis and accumulation, which seems to lag behind VOC production. Further genetic and molecular investigation is needed to identify specific VOC signaling molecules, their receptors, and their mode of action under N-starvation conditions.

DATA AVAILABILITY STATEMENT

The raw data supporting the conclusions of this article will be made available by the authors, without undue reservation, to any qualified researcher.

AUTHOR CONTRIBUTIONS

PK and IK-G conceived the research. PK performed all experimental work, data analysis, and wrote the first draft of the manuscript. AC and VT contributed to the analysis of volatiles. SD-C performed the fatty acid analysis and assisted in growth experiments. IK-G reviewed and edited the manuscript and supervised the project. All authors read, edited, and approved the final manuscript.

FUNDING

This work was supported by a grant from the Ministry of Science, Technology and Space, Israel (grant number 3-12422).

ACKNOWLEDGMENTS

PK and AC acknowledged the Blaustein Postdoctoral Fellowship from the Blaustein Center for Scientific Cooperation (BGU). We are grateful to Noga Sikron Peres for her help with the GC-MS analysis. VT was the chair of Sonnenfeldt-Goldman Career Development in Desert Research.

SUPPLEMENTARY MATERIAL

The Supplementary Material for this article can be found online at: https://www.frontiersin.org/articles/10.3389/fmars.2020.00410/full#supplementary-material

REFERENCES

Achyuthan, K. E., Harper, J. C., Manginell, R. P., and Moorman, M. W. (2017). Volatile metabolites emission by in vivo microalgae-an overlooked opportunity? *Metabolites* 7, 1–14. doi: 10.3390/metabo7030039

Ahn, H. M., Kim, S., Hyun, S., Lim, S. R., Kim, H., Oh, J., et al. (2016). Effects of the timing of a culture temperature reduction on the comprehensive metabolite profiles of *Chlorella vulgaris*. *J. Appl. Phycol.* 28, 2641–2650. doi: 10.1007/s10811-016-0817-4

Akakabe, Y., Matsui, K., and Kajiwara, T. (2003). 2,4-Decadienals are produced via (R)-11-HPITE from arachidonic acid in marine green alga Ulva conglobata. Bioorg. *Med. Chem.* 11, 3607–3609. doi: 10.1016/s0968-0896(03)00364-x

Ameye, M., Allmann, S., Verwaeren, J., Smagghe, G., Haesaert, G., Schuurink, R. C., et al. (2018). Green leaf volatile production by plants: a meta-analysis. *New Phytol.* 220, 666–683. doi: 10.1111/nph.14671

Andreou, A., and Feussner, I. (2009). Lipoxygenases-structure and reaction mechanism. *Phytochemistry* 70, 1504–1510. doi: 10.1016/j.phytochem.2009.05.008

Babushok, V. I., Linstrom, P. J., and Zenkevich, I. G. (2011). Retention indices for frequently reported compounds of plant essential oils. *J. Phys. Chem. Ref. Data* 40:043101. doi: 10.1063/1.3653552

Berger, R. G. (2009). Biotechnology of flavours - the next generation. *Biotechnol. Lett.* 31, 1651–1659. doi: 10.1007/s10529-009-0083-5

Bernard, A., Domergue, F., Pascal, S., Jetter, R., Renne, C., Faure, J. D., et al. (2012). Reconstitution of plant alkane biosynthesis in yeast demonstrates that *Arabidopsis* ECERIFERUM1 and ECERIFERUM3 are core components of a very-long-chain alkane synthesis complex. *Plant Cell* 24, 3106–3118. doi: 10.1105/tpc.112.099796

Bigogno, C., Khozin-Goldberg, I., and Cohen, Z. (2002). Accumulation of arachidonic acid-rich triacylglycerols in the microalga *Parietochloris incisa* (*Trebouxiophyceae*. *Chlorophyta*). *Phytochemistry* 60, 135–143. doi: 10.1016/s0031-9422(02)00037-7

Boonprab, K., Matsui, K., Akakabe, Y., Yotsukura, N., and Kajiwara, T. (2019). 11-Hydroperoxide eicosanoid-mediated 2(E),4(E)-decadienal production from arachidonic acid in the brown algae, *Saccharina angustata*. *J. Appl. Phycol.* 31, 2719–2727. doi: 10.1007/s10811-019-01776-y

Chen, H., Yang, R., Chen, J., Luo, Q., Cui, X., Yan, X., et al. (2019). 1-Octen-3-ol, a self-stimulating oxylipin messenger, can prime and induce defense of marine alga. *BMC Plant Biol.* 19:37. doi: 10.1186/s12870-019-1642-0

Chong, J., Wishart, D. S., and Xia, J. (2019). Using Metaboanalyst 4.0 for comprehensive and integrative metabolomics data analysis. *Curr. Protoc. Bioinformatics* 68:e86. doi: 10.1002/cpbi.86

de Alencar, D. B., Diniz, J. C., Rocha, S. A. S., Pires-Cavalcante, K. M. S., Freitas, J. O., Nagano, C. S., et al. (2017). Chemical composition of volatile compounds in two red seaweeds, *Pterocladiella capillacea* and *Osmundaria obtusiloba*, using static headspace gas chromatography mass spectrometry. *J. Appl. Phycol.* 29, 1571–1576. doi: 10.1007/s10811-016-1020-3

Djian, B., Hornung, E., Ischebeck, T., and Feussner, I. (2019). The green microalga Lobosphaera incisa harbours an arachidonate 15S-lipoxygenase. *Plant Biol.* 21(Suppl. 1), 131–142. doi: 10.1111/plb.12920

Du, Z. Y., Lucker, B. F., Zienkiewicz, K., Miller, T. E., Zienkiewicz, A., Sears, B. B., et al. (2018). Galactoglycerolipid lipase PGD1 is involved in thylakoid membrane remodeling in response to adverse environmental conditions in Chlamydomonas. *Plant Cell* 30, 447–465. doi: 10.1105/tpc.17.00446

Durme, J. V., Goiris, K., Winne, A., Cooman, L., and Muylaert, K. (2013). Evaluation of the volatile composition and sensory properties of five species of microalgae. *J. Agric. Food Chem.* 61, 10881–10890. doi: 10.1021/jf403112k

Fink, P. (2007). Ecological functions of volatile organic compounds in aquatic systems. *Mar. Freshw. Behav. Physiol.* 40, 155–168. doi: 10.1080/10236240701602218

Goodner, K. L. (2008). Practical retention index models of OV-101, DB-1, DB-5, and DB-Wax for flavor and fragrance compounds. *LWT Food Sci. Technol.* 41, 951–958. doi: 10.1016/j.lwt.2007.07.007

Gutbrod, K., Romer, J., and Dörmann, P. (2019). Phytol metabolism in plants. *Prog. Lipid Res.* 74, 1–17. doi: 10.1016/j.plipres.2019.01.002

Halliwell, B., and Gutteridge, J. M. C. (1999). *Free Radicals in Biology and Medicine*, 3rd Edn. Oxford: Oxford University Press.

Hosoglu, M. I. (2018). Aroma characterization of five microalgae species using solid-phase microextraction and gas chromatography–mass spectrometry/olfactometry. *Food Chem.* 240, 1210–1218. doi: 10.1016/j.foodchem.2017.08.052

Jacob-Lopes, E., and Franco, T. T. (2013). From oil refinery to microalgal biorefinery. *J. CO2 Util.* 2, 1–7. doi: 10.1016/j.jcou.2013.06.001

Jacob-Lopes, E., Scoparo, C. H. G., Queiroz, M. I., and Franco, T. T. (2010). Biotransformations of carbon dioxide in photobiorreactors. *Energ. Convers. Manag.* 51, 894–900. doi: 10.1007/s11274-013-1254-z

Jerković, I., Marijanović, Z., Roje, M., Kuś, P. M., Jokić, S., and ÈozÏ-Rakovac, R. (2018). Phytochemical study of the headspace volatile organic compounds of fresh algae and seagrass from the Adriatic Sea (single point collection). *PLoS One* 13:e0196462. doi: 10.1371/journal.pone.0196462

Kalyanaraman, B., Darley-Usmar, V., Davies, K. J., Dennery, P. A., Forman, H. J., Grisham, M. B., et al. (2012). Measuring reactive oxygen and nitrogen species with fluorescent probes: challenges and limitations. *Free Radic Biol Med.* 52, 1–6. doi: 10.1016/j.freeradbiomed.2011.09.030

Kessler, A., Halitschke, R., Diezel, C., and Baldwin, I. T. (2006). Priming of plant defense responses in nature by airborne signaling between Artemisia tridentate and Nicotiana attenuate. *Oecologia* 148, 280–292. doi: 10.1007/s00442-006-0365-8

Khozin-Goldberg, I., Leu, S., and Boussiba, S. (2016). "Microalgae as a source for VLC-PUFA production," in *Lipids in Plant and Algae Development, Subcellular Biochemistry*, eds N. Yuki, and L. B. Yonghua, (Cham: Springer), 471–510. doi: 10.1007/978-3-319-25979-6_19

Kihara, H., Tanaka, M., Yamato, K. T., Horibata, A., Yamada, A., Kita, S., et al. (2014). Arachidonic acid-dependent carbon-eight volatile synthesis from wounded liverwort (*Marchantia polymorpha*). *Phytochemistry* 107, 42–49. doi: 10.1016/j.phytochem.2014.08.008

Kokabi, K., Gorelova, O., Ismagulova, T., Itkin, M., Malitsky, S., Boussiba, S., et al. (2019). Metabolomic foundation for differential responses of lipid metabolism to nitrogen and phosphorus deprivation in an arachidonic acid-producing green microalga. *Plant Sci.* 283, 95–115. doi: 10.1016/j.plantsci.2019.02.008

Kugler, A., Zorin, B., Didi-Cohen, S., Sibiryak, M., Gorelova, O., Ismagulova, T., et al. (2019). Long-chain polyunsaturated fatty acids in the green microalga *Lobosphaera incisa* contribute to tolerance to abiotic stresses. *Plant Cell Physiol.* 60, 1205–1223. doi: 10.1093/pcp/pcz013

Kumari, P. (2017). "Seaweed lipidomics in the era of 'omics' biology- a contemporary perspective," in *System Biology of Marine Ecosystems*, eds M. Kumar, and P. Ralph, (Cham: : Springer), 49–97. doi: 10.1007/978-3-319-62094-7_4

Lafarge, C., and Cayot, N. (2019). Insight on a comprehensive profile of volatile compounds of *Chlorella vulgaris* extracted by two "green" methods. *Food Sci. Nutr.* 7, 918–929. doi: 10.1002/fsn3.831

Liu, R., Zhu, F., Lu, L., Fu, A., Lu, J., Deng, Z., et al. (2014). Metabolic engineering of fatty acyl-ACP reductase-dependent pathway to improve fatty alcohol production in *Escherichia coli*. *Metab. Eng.* 22, 10–21. doi: 10.1016/j.ymben.2013.12.004

Meskhidze, N., Sabolis, A., Reed, R., and Kamykowski, D. (2015). Quantifying environmental stress-induced emissions of algal isoprene and monoterpenes using laboratory measurements. *Biogeosciences* 12, 637–651. doi: 10.5194/bg-12-637-2015

Moelzner, J., and Fink, P. (2015). Consumer patchiness explained by volatile infochemicals in a freshwater ecosystem. *Ecosphere* 6, 1–15. doi: 10.1890/ES14-00246.1

Nagappan, S., Devendran, S., Tsaic, P., Jayaramana, H., Alagarsamya, V., Pugazhendhid, A., et al. (2020). Metabolomics integrated with transcriptomics and proteomics: evaluation of systems reaction to nitrogen deficiency stress in microalgae. *Process Biochem.* 91, 1–14. doi: 10.1016/j.procbio.2019.11.027

Pal-Nath, D., Didi-Cohen, S., Shtaida, N., Nath, P. R., Samani, T., Boussiba, S., et al. (2017). Improved productivity and oxidative stress tolerance under nitrogen starvation is associated with the ablated Δ5 desaturation in the green microalga Lobosphaera incisa. *Algal Res.* 26, 25–38. doi: 10.1016/j.algal.2017.06.026

Pal-Nath, D., Khozin-Goldberg, I., Cohen, Z., and Boussiba, S. (2011). The effect of light, salinity, and nitrogen availability on lipid production by *Nannochloropsis* sp. *Appl. Microbiol. Biotechnol.* 90, 1429–1441. doi: 10.1007/s00253-011-3170-1

Rontania, J., and Volkman, J. K. (2003). Phytol degradation products as biogeochemical tracers in aquatic environments. *Org. Geochem.* 34, 1–35. doi: 10.1016/s0146-6380(02)00185-7

Rowland, O., and Domergue, F. (2012). Plant fatty acyl reductases: enzymes generating fatty alcohols for protective layers with potential for industrial applications. *Plant Sci.* 193-194, 28–38. doi: 10.1016/j.plantsci.2012.05.002

Sabharwal, T., Sathasivan, K., and Mehdy, M. C. (2017). Defense related decadienal elicits membrane lipid remodeling in the diatom *Phaeodactylum tricornutum*. *PLoS One* 12:e0178761. doi: 10.1371/journal

Santos, A. B., Vieira, K. R., Nogara, G. P., Wagner, R., Jacob-Lopes, E., and Zepka, L. Q. (2016). "Biogeneration of volatile organic compounds by microalgae: occurrence, behavior, ecological implications and industrial applications," in *Volatile Organic Compounds*, ed. J. P. Moore, (New York, NY: Nova Science Publishers, Inc), 1–24.

Siegler, H., Valerius, O., Ischebeck, T., Popko, J., Tourasse, N. J., Vallon, O., et al. (2017). Analysis of the lipid body proteome of the oleaginous alga *Lobosphaera incisa*. *BMC Plant Biol.* 17:98. doi: 10.1186/s12870-017-1042-2

Solovchenko, A., Merzlyak, M. N., Khozin-Goldberg, I., Cohen, Z., and Boussiba, S. (2010). Coordinated carotenoid and lipid syntheses induced in *Parietochloris incisa* (*Chlorophyta*, *Trebouxiophyceae*) mutant deficient in Δ5 desaturase by nitrogen starvation and high light. *J. Phycol.* 46, 763–772. doi: 10.1111/j.1529-8817.2010.00849.x

Solovchenko, A., Solovchenko, O., Khozin-Goldberg, I., Didi-Cohen, S., Pal-Nath, D., Cohen, Z., et al. (2013). Probing the effects of high-light stress on pigment and lipid metabolism in nitrogen-starving microalgae by measuring chlorophyll fluorescence transients: studies with a Δ5 desaturase mutant of *Parietochloris incisa* (*Chlorophyta*, *Trebouxiophyceae*). *Algal Res.* 2, 175–182. doi: 10.1016/j.algal.2013.01.010

Solovchenko, A. E. (2012). Physiological role of neutral lipid accumulation in eukaryotic microalgae under stresses. *Russ. J. Plant Physiol.* 59, 167–176. doi: 10.1134/S1021443713010081

Song, Y., Zhao, J., Chen, J., Luo, Q., Yang, R., Xu, J., et al. (2018). Heat shock-induced metabolic conversion of membrane lipids, fatty acids and volatile organic compounds of *Pyropia haitanensis* under different heat shock time. *Phycol. Res.* 66, 89–99. doi: 10.1111/pre.12206

Sorigué, D., Légeret, B., Cuiné, S., Blangy, S., Moulin, S., Billon, E., et al. (2017). An algal photoenzyme converts fatty acids to hydrocarbons. *Science* 357, 903–907. doi: 10.1126/science.aan6349

Sorigué, D., Légeret, B., Cuiné, S., Morales, P., Mirabella, B., Guédeney, G., et al. (2016). Microalgae synthesize hydrocarbons from long-chain fatty acids via a light-dependent pathway. *Plant Physiol.* 171, 2393–2405. doi: 10.1104/pp.16.00462

Vioque, J., and Kolattukudy, P. E. (1997). Resolution and purification of an aldehyde-generating and an alcohol-generating fatty acyl-coA reductase from pea leaves (*Pisum sativum* L.). *Arch. Biochem. Biophys.* 340, 64–72. doi: 10.1006/abbi.1997.9932

vom Dorp, K., Hölzl, G., Plohmann, C., Eisenhut, M., Abraham, M., Weber, A. P., et al. (2015). Remobilization of phytol from chlorophyll degradation is essential for tocopherol synthesis and growth of *Arabidopsis*. *Plant Cell* 27, 2846–2859. doi: 10.1105/tpc.15.00395

Wang, J., Zhu, J., Liu, S., Liu, B., Gao, Y., and Wu, Z. (2011). Generation of reactive oxygen species in cyanobacteria and green algae induced by allelochemicals of submerged macrophytes. *Chemosphere* 85, 977–982. doi: 10.1016/j.chemosphere.2011.06.076

Wang, X., and Kolattukudy, P. E. (1995). Solubilization and purification of aldehyde-generating fatty acyl-CoA reductase from green alga Botryococcus braunii. *FEBS Lett.* 370, 15–18. doi: 10.1016/0014-5793(95)00781-4

Wichard, T., Poulet, S. A., Halsband-Lenk, C., Albaina, A., Harris, R., Liu, D., et al. (2005). Survey of the chemical defence potential of diatoms: screening of fifty species for α,β,γ,δ-unsaturated aldehydes. *J. Chem. Ecol.* 31, 949–958. doi: 10.1007/s10886-005-3615-z

Zheng, Y., Li, L., Liu, Q., Yang, J., Wang, X., Liu, W., et al. (2012). Optimization of fatty alcohol biosynthesis pathway for selectively enhanced production of C12/14 and C16/18 fatty alcohols in engineered *Escherichia coli*. *Microb. Cell Fact.* 11:65. doi: 10.1186/1475-2859-11-65

Zhou, L., Chen, J., Xu, J., Li, Y., Zhou, C., and Yan, X. (2017). Change of volatile components in six microalgae with different growth phases. *J. Sci. Food. Agric.* 97, 761–769. doi: 10.1002/jsfa.7794

Zhu, Z.-J., Chen, H.-M., Chen, J.-J., Yang, R., and Yan, X.-J. (2018). One-step bioconversion of fatty acids into C8–C9 volatile aroma compounds by a multifunctional lipoxygenase cloned from *Pyropia haitanensis*. *J. Agric. Food Chem.* 66, 1233–1241. doi: 10.1021/acs.jafc.7b05341

Zuo, Z. (2019). Why algae release volatile organic compounds—the emission and roles. *Front. Microbiol.* 10:491. doi: 10.3389/fmicb.2019.00491

Zuo, Z., Chen, Z., Zhu, Y., Bai, Y., and Wang, Y. (2015). Reactive oxygen species contribute to the release of volatile organic compounds from *Chlamydomonas reinhardtii* during programmed cell death. *Phycol. Res.* 63, 37–42. doi: 10.1111/pre.12071

Zuo, Z., Zhu, Y., Bai, Y., and Wang, Y. (2012a). Acetic acid-induced programmed cell death and release of volatile organic compounds in *Chlamydomonas reinhardtii*. *Plant Physiol. Biochem.* 51, 175–184. doi: 10.1016/j.plaphy.2011.11.003

Zuo, Z., Zhu, Y., Bai, Y., and Wang, Y. (2012b). Volatile communication between *Chlamydomonas reinhardtii* cells under salt stress. *Biochem. Syst. Ecol.* 40, 19–24. doi: 10.1016/j.bse.2011.09.007

Conflict of Interest: The authors declare that the research was conducted in the absence of any commercial or financial relationships that could be construed as a potential conflict of interest.

Copyright © 2020 Kumari, Cna'ani, Didi-Cohen, Tzin and Khozin-Goldberg. This is an open-access article distributed under the terms of the Creative Commons Attribution License (CC BY). The use, distribution or reproduction in other forums is permitted, provided the original author(s) and the copyright owner(s) are credited and that the original publication in this journal is cited, in accordance with accepted academic practice. No use, distribution or reproduction is permitted which does not comply with these terms.